Global Change Biology

Global Change Biology (2010) **16**, 617–640, doi: 10.1111/j.1365-2486.2009.01997.x

Implications of future climate and atmospheric CO_2 content for regional biogeochemistry, biogeography and ecosystem services across East Africa

RUTH M. DOHERTY*, STEPHEN SITCH†‡, BENJAMIN SMITH§, SIMON L. LEWIS¶ and PHILIP K. THORNTON*‖

*School of GeoSciences, Crew Building, Kings Buildings, University of Edinburgh, Edinburgh EH9 3JN, UK, †Met Office Hadley Centre, JCHMR, Maclean Building, Wallingford OX10 8BB, UK, ‡School of Geography, University of Leeds LS2 9JT, UK, §Department of Physical Geography and Ecosystems Analysis, Lund University Sölvegatan 12, 22362 Lund, Sweden, ¶Earth & Biosphere Institute, School of Geography, University of Leeds, Leeds LS2 9JT, UK, ‖International Livestock Research Institute, P.O. Box 30709, Nairobi 00100, Kenya

Abstract

We model future changes in land biogeochemistry and biogeography across East Africa. East Africa is one of few tropical regions where general circulation model (GCM) future climate projections exhibit a robust response of strong future warming and general annual-mean rainfall increases. Eighteen future climate projections from nine GCMs participating in the Intergovernmental Panel on Climate Change (IPCC) Fourth Assessment were used as input to the LPJ dynamic global vegetation model (DGVM), which predicted vegetation patterns and carbon storage in agreement with satellite observations and forest inventory data under the present-day climate. All simulations showed future increases in tropical woody vegetation over the region at the expense of grasslands. Regional increases in net primary productivity (NPP) (18–36%) and total carbon storage (3–13%) by 2080–2099 compared with the present-day were common to all simulations. Despite decreases in soil carbon after 2050, seven out of nine simulations continued to show an annual net land carbon sink in the final decades of the 21st century because vegetation biomass continued to increase. The seasonal cycles of rainfall and soil moisture show future increases in wet season rainfall across the GCMs with generally little change in dry season rainfall. Based on the simulated present-day climate and its future trends, the GCMs can be grouped into four broad categories. Overall, our model results suggest that East Africa, a populous and economically poor region, is likely to experience some ecosystem service benefits through increased precipitation, river runoff and fresh water availability. Resulting enhancements in NPP may lead to improved crop yields in some areas. Our results stand in partial contradiction to other studies that suggest possible negative consequences for agriculture, biodiversity and other ecosystem services caused by temperature increases.

Keywords: climate change, climate uncertainty, DGVM, dynamic global vegetation models, East Africa, ecosystem services, general circulation models, regional climate impacts

Received 29 January 2009 and accepted 10 May 2009

Introduction

Tropical ecosystems are of particular importance within the global carbon cycle because of the large amount of carbon stored in undisturbed tropical forests [40% of global biomass, >60% of global net primary productivity (NPP); Denman *et al*., 2007]. Changes in the carbon balance of these regions could have significant effects on atmospheric carbon dioxide (CO_2) concentrations (Lewis, 2006; Denman *et al*., 2007).

Impacts of future climate change on biogeography and the carbon cycle have been studied using dynamic global vegetation models (DGVMs) driven by projections of future climate, typically generated by coupled

Correspondence: R. M. Doherty, e-mail: Ruth.Doherty@ed.ac.uk

atmosphere-ocean general circulation models (hereinafter 'GCMs') for a given future greenhouse gas emissions trajectory or scenario (e.g. Cramer *et al*., 2001; Schaphoff *et al*., 2006). Uncertainties in the resulting projections of terrestrial carbon storage are large and stem from the use of different future emissions and land-use scenarios, the range of climate projections simulated by different GCMs for a particular emissions scenario, the representation and parameterisation of key ecosystem processes (Zaehle *et al*., 2005), and carbon cycle feedbacks on climate (Friedlingstein *et al*., 2006; Sitch *et al*., 2008).

A number of DGVM studies have simulated the effect of rising CO_2 concentrations alone on global terrestrial carbon uptake. CO_2 'fertilisation' due to biochemical enhancement of photosynthesis and improved water-use efficiency lead to increased productivity and vegetation growth in models (Hickler *et al*., 2008) and many field experiments (Norby *et al*., 2005). This increase is generally reduced when climate change is accounted for (e.g., Cramer *et al*., 2001; Cox *et al*., 2004; Berthelot *et al*., 2005). However, Schaphoff *et al*. (2006) found that the spread in future climate projections among five GCMs for the same emissions scenario led to large differences in DGVM-predicted global terrestrial carbon storage, including differences in the sign of the global trend. Much of this variability is associated with certain tropical regions, where reduced hydrological cycling may amplify drying trends – a positive feedback of vegetation changes to climate (e.g., Friedlingstein *et al*., 2006).

One region of the tropics where GCMs show a relatively robust response across models is East Africa (Hulme *et al*., 2001; Ruosteenoja *et al*., 2003; Christensen *et al*., 2007). Among the GCMs included in an A1B climate change experiment in the latest IPCC Fourth Assessment (IPCC-AR4), all show increases in temperature for East Africa (18°N-12°S, 22–52°E) that are larger than the global average response in all seasons. Eighteen out of the 21 models project a rainfall increase in the core of this region, east of the Great Lakes (Christensen *et al*., 2007). This regional pattern is consistent with the large-scale picture in a high-CO_2 climate of drying in much of the subtropics and an increase (or little change) in precipitation in the tropics, increasing the rainfall gradients (Christensen *et al*., 2007).

We use a DGVM to simulate future changes in land carbon cycling and biogeography across East Africa. The East African region is selected for three reasons. Firstly, as discussed above, both simulated temperature and rainfall trends are generally similar across the IPCC-AR4 GCMs, allowing a test of whether robust statements about the ecosystem response are possible for regions where GCMs are in qualitative agreement. Secondly, the impact of a warmer but wetter future climate on the structure and functioning of tropical ecosystems has not been fully evaluated since previous DGVM-based studies of tropical regions have typically focused on the consequences of increased aridity associated with climate change (Cox *et al*., 2000, 2004; Friedlingstein *et al*., 2006). Thirdly, despite the importance of tropical ecosystems for the global carbon cycle, relatively few modelling studies have focused on the response of African tropical ecosystems to climate change. The East Africa region provides critically important ecosystem services for its human population of more than 160 million (GRUMP, 2005), notably agriculture and livestock feed, while the forest and savannah vegetation provide the basis for significant income from tourism.

Materials and methods

LPJ model

This study uses the Lund–Potsdam–Jena (LPJ) DGVM to simulate changes in vegetation and ecosystem carbon cycling under future climate conditions. The model version designated LPJv1.2 was used, as originally described by Sitch *et al*. (2003), with improved representations of ecosystem hydrology as documented by Gerten *et al*. (2004). LPJv1.2 (hereinafter 'LPJ') is a process-based biogeography–biogeochemistry model that simulates the spatio-temporal dynamics of terrestrial vegetation together with land-atmosphere carbon and water exchanges. A coupled photosynthesis-hydrological scheme computes gross primary productivity, plant respiration, and evapotranspiration on a daily time step based on the current climate, atmospheric CO_2 concentration, vegetation structure and phenological state, and soil water content. Carbon accrued by plants in the course of 1 year – i.e. the NPP – is allocated to the living tissue compartments leaves, sapwood, and fine roots according to a set of allometric and functional rules. Leaf and root turnover redistribute carbon to litter and soil organic matter carbon pools. Decomposition is sensitive to soil temperature and moisture, and results in the return of soil carbon to the atmosphere as heterotrophic respiration (R_h). The vegetation of each simulated area ('grid cell') is represented as a mixture of generalised plant functional types (PFTs) that compete for water, light, and space. PFTs are differentiated by their bioclimatic, physiological (C_3 or C_4 photosynthesis), physiognomic (woody or herbaceous), phenological (deciduous or evergreen), and flammability characteristics (Table 1). Disturbance by wildfire is simulated prognostically based on climate and vegetation structure (Thonicke *et al*., 2001). Vegetation structure and composition in terms of PFTs adjust

Table 1 Parameters distinguishing the seven plant functional types (PFTs) simulated by LPJ within the climate space of the East African study area

			Plant functional type*						
Parameter	Symbol	Units	TrBE	TrBR	TeNE	TeBE	TeBS	C3G	C4G
Physiognomy									
Growth form*			W	W	W	W	W	H	H
Foliar physiognomy*			B	B	N	B	B	G	G
Fraction of roots in upper/lower soil layer†		%	85/15	60/40	60/40	70/30	70/30	80/20	80/20
Bioclimate									
Minimum coldest-month temperature for survival	$T_{c,min}$	°C	15.5	15.5	3.0	3.0	−17.0	–	15.5
Maximum coldest-month temperature for establishment	$T_{c,max}$	°C	–	–	18.8	18.8	15.5	15.5	–
Minimum degree-day sum (5 °C base) for establishment	GDD_5	°C day^{-1}	–	–	1200	1200	1200	–	–
Phenology									
Foliar phenology type*			E	R	E	E	S	E/R/S	E/R/S
Foliar turnover rate	f_{leaf}	year^{-1}	0.5	1.0	0.25	1.0	1.0	1.0	1.0
Fine root turnover rate	f_{root}	year^{-1}	1.0	1.0	0.25	1.0	1.0	0.5	0.5
Physiology									
Photosynthetic pathway			C_3	C_3	C_3	C_3	C_3	C_3	C_4
Optimum temperature range for photosynthesis		°C	25–30	25–30	20–30	20–30	20–25	10–30	20–45
Tissue respiration rate at 10 °C	R	g C g N day^{-1}	0.011	0.011	0.066	0.066	0.066	0.066	0.011
Minimum canopy conductance	g_{min}	mm s^{-1}	0.5	0.5	0.3	0.5	0.5	0.5	0.5
Maximum evapotranspiration rate	E_{max}	mm day^{-1}	7	7	5	5	5	5	7
Soil moisture content below which leaves fall				0.2				0.1	0.1
Fire									
Moisture of extinction	ME	frac	0.35	0.35	0.35	0.35	0.35	0.35	0.35

*TrBE, tropical broadleaved evergreen; TrBR, tropical broadleaved raingreen; TeNE, temperate needleleaved evergreen; TeBE, temperate broadleaved evergreen; TeBS, temperate broadleaved summergreen; W, woody; H, herbaceous; B, broadleaf; N, needleleaf; G, grass; E, evergreen; R, raingreen; S, summergreen.
†0–50 cm/50–200 cm.

Table 2 Model name, developing institution and spatial resolution of the nine IPCC AR4 GCMs used in this study

		Spatial resolution (°)				
Centre	Model name	Longitude	Latitude	Time span	Ensembles	Forcings 20C3M/A2
NCAR, USA	CCSM3	~ 1.41	~ 1.41	1860–2099	5	G, A, V/G, A
CCCma, Canada	CGCM3.1	~ 3.75	~ 3.75	1850–2100	5	G, A, G, A
CNRM, France	CNRM CM3	~ 2.8	~ 2.8	1860–2099	1	G, A/G, A
CSIRO, Australia	CSIRO MK3.0	~ 1.875	~ 1.875	1871–2100	1	G, A/G, A
MPI, Germany	ECHAM5	~ 1.875	~ 1.875	1860–2100	3	G, A/G, A
GFDL, USA	GFDL CM2.1	2.5	2.0	1861–2100	1	G, A, S, V, L/G, A
Hadley Centre, UK	HadCM3	3.75	2.5	1860–2099	1	G, A, S, V/G, A
Hadley Centre, UK	HadGEM1	1.875	1.25	1860–2098	1	G, A, S, V, L/G, A
MRI, Japan	CGCM2 3 (MRI)	~ 2.8	~ 2.8	1850–2099	1	G, A, S, V/G, A

Time periods and forcing used in the 20C3M and SRESA2 scenario.
G, greenhouse gases (GHG); A, aerosol; S, solar; V, volcanic; L, land-use; ~ , spectral resolution models.

dynamically to changes in climate and CO_2 so that transient carbon balances are simulated on multiannual to centennial time-scales. The model version we used simulates potential natural vegetation and does not include agriculture or managed forests or the effects of human activities on the landscape. LPJ has been extensively validated in comparison to observations of terrestrial biogeochemistry and biogeography (e.g., Sitch *et al.*, 2003; Cramer *et al.*, 2004; Gerten *et al.*, 2004; Morales *et al.*, 2005; Zaehle *et al.*, 2005; Schaphoff *et al.*, 2006).

Driving climate, atmospheric CO_2 concentrations and soils

LPJ requires monthly climate (temperature, precipitation, cloud cover), atmospheric CO_2 concentration and soil texture as input data. Multimodel climate projections for the period 1850–2100 were obtained from GCM simulations performed for IPCC–AR4. These data were acquired from the Programme for Climate Model Diagnosis and Inter-comparison (PCMDI) website (http://www-pcmdi.llnl.gov). Results from 18 GCM simulations and two 'experiments' were used. The 'Climate of the 20th century experiment' (20C3M) covered the period 1850–1990. The 'SRES A2' experiment extended the 20C3M experiment up to 2100. The A2 experiment, which is based on the assumptions of slow technological change, high population growth, and regionally oriented economic growth (Nakicenovic & Swart, 2000) was selected for this study because it is associated with one of the more extreme emissions scenarios, resulting in larger simulated changes in climate than the SRES A1B, B1 and B2 scenarios. Hence, the LPJ simulations driven with SRES A2 climate projections should produce more extreme ecosystem responses than those performed using climate derived from the other aforementioned scenarios. Total anthropogenic CO_2 emissions increase from 8.0 Pg C yr^{-1} in 2000 to 29.1 Pg C yr^{-1} by 2100 (IPCC, 2001, Appendix II); atmospheric CO_2 concentrations reach 715 ppm by the 2080s (Nakicenovic & Swart, 2000). In 20C3M, anthropogenic (greenhouse gases, aerosols) and for some GCMs natural (solar, volcanoes, land-use) forcings (Table 2) were used in order to produce the most realistic model descriptions of the observed historical climate. The 18 GCM simulations (Table 2) encompass nine different models (multi-member ensembles were available for three GCMs); they represent all available archived GCM data for the above experiments that include the relevant driving climate variables for LPJ.

In order to quantify uncertainty propagating from differences among GCM climate projections we use GCM-generated climate data directly as input data to LPJ. The station-based CRU TS 2.1 (hereafter CRU05) gridded dataset for 1901–2002 (New *et al.*, 2000) was used to provide a comparison with GCM projections over the 20th century as well as input data to a 'baseline' 20th century simulation with LPJ.

For the period 1850–1990, we used annually varying atmospheric CO_2 concentrations derived from atmospheric and ice-core measurements (Keeling *et al.*, 1995; Etheridge *et al.*, 1996) as input to LPJ. For 1990–2100, annual values for the SRES A2 scenario, calculated by the Bern-CC global carbon cycle model, were used (IPCC, 2001, Appendix II). Soil texture classes were based on a combination of the Zobler (1986) and the FAO databases (FAO, 1991) as described by Sitch *et al.* (2003), re-calculated from the original $0.5 \times 0.5^\circ$ grid to the resolution of the individual GCM.

LPJ simulations were performed at the individual GCM grid resolution, ranging from ~ 1.4° to 3.75° (Table 2). LPJ was initialised by means of an initial 1000-year 'spin-up' using a repeat cycle of the first 30-years of the driving climate time series to obtain vegetation and soil carbon pools in an approximate

steady-state at the beginning of the subsequent climate change experiment (1850 for all GCM-driven experiments; 1901 for the CRU05-driven historical simulation). Only the transient period from 1850 to 2100 (1901–2002 for CRU05) was subsequently analysed.

Study region and validation data

The study region is defined as the window bounded by 12.5°N, 12.5°S, 25°E and 42.5°E representing the whole of East Africa (Kenya, Tanzania, Uganda, Rwanda, Burundi, Ethiopia, Somalia) and parts of central Africa (Democratic Republic of Congo [DRC] and southern Sudan).

While a comprehensive validation of the DGVM would be beyond the scope of this study, we compared simulated vegetation patterns and biomass carbon storage for the recent past against two satellite-derived vegetation distribution maps and biomass carbon derived from forest inventory plot data. The satellite products from MODIS-Terra for 2001 (Friedl *et al*., 2002) and GLC2000 (JRL, 2005) were used for the spatial vegetation distribution comparison.

The forest inventory data consisted of published carbon storage estimates from intact forests (Lewis *et al*., 2009) and unpublished tree diameter data from 34 monitoring plots (67 ha in total) in nine $0.5 \times 0.5^\circ$ grid squares located in DRC, Uganda and Tanzania. These intact forests plots were deliberately located to avoid significant direct human impacts and are therefore likely to be close to the natural potential vegetation modelled in the study.

The tree diameter data were converted to aboveground carbon stocks using an allometric equation with parameters based on destructive sampling in moist forest (Chave *et al*., 2005). Tissue density of each species was obtained from a compilation of published sources (Chave *et al*., 2009), a biomass carbon density of 50% (Chave *et al*., 2005, 2009; Lewis *et al*., 2009), and a root : shoot ratio of 0.25 were assumed (Deans *et al*., 1996; Lewis *et al*., 2009).

Present-day and future climate projections

Following the convention in IPCC-AR4, results for the period 1981–2000 were averaged to derive anomalies from the 'present-day' mean. Averaged across the East African region, the CRU05 observations show a rise in annual-mean temperature of $\sim 0.5\,^\circ$C between 1901 and 2002. CRU05 precipitation exhibits considerable inter-decadal variability over the 20th century (Fig. 1). The wet period in the 1960s is well-documented (e.g. Conway, 2002).

Six of the nine GCMs underestimate annual-average temperatures over the 1981–2000 period in this region by 1.2° (multimodel median) compared with CRU05 (Fig. 1a, Table 3). Simulated temperatures from ECHAM5, HadCM3 and CCSM3 are in good agreement with the CRU05 gridded observations (Table 3). Annual-mean temperatures rise by 2.3–3 °C (Fig. 1b, 12–20%; Table 3) by 2080–2100 relative to 1981–2000. Conversely, most GCMs overestimate 20th century annual-average precipitation averaged across East Africa compared with CRU05 (Fig. 1c; Table 3). GFDL, CSIRO and HADGEM1 results exhibit the closest agreement to observations (Fig. 1c; Table 3) and hence are among the drier models. The remaining five GCMs are wetter by 0.5–1.8 mm day^{-1} (Table 3, Fig. 1b), with the exception of ECHAM5 where annual-average precipitation is underestimated by 0.4 mm day^{-1}. Seven of the nine GCMs show an increasing precipitation trend from the 1990s onwards (Fig. 1b and d; 6–21% in 2080–2099; Table 3). We classify the nine GCMs into four broad categories based on the simulated present-day climate and its future evolution (Fig. 1) as compared with the GCM average. These are:

Group 1: Warmer, wetter models that generally exhibit positive future trends in temperature and rainfall: MRI, CCSM3 and HadCM3 (red curves in Fig. 1). The climate simulated by CCSM3 and HadCM3 is among the warmest – in closest agreement (along with ECHAM5) with CRU05 observations and is fairly wet. MRI projects an East African climate with high rainfall over the 20th century and mid-range to high temperatures. CCSM3 and HadCM3 exhibit steep future warming trends (Fig. 1b; Table 3), while MRI exhibits a more moderate warming trend. All three GCMs exhibit a positive trend in precipitation (Fig. 1d) with the CCSM3 ensembles depicting the steepest trend ($\sim$ 20% increase between 2080–2099 and 1981–2000, Table 3).

Group 2: Cooler, wetter models that exhibit strong positive future trends in temperature and rainfall: CNRM and CGCM3 (blue curves). These two GCMs project the coldest temperatures but have the highest precipitation (together with MRI) over the East African region. Increases both in temperature (16–20%) and precipitation (10–12%) by 2080–2099 are among the largest across the GCMs (Table 3).

Group 3: Fairly warm and moderately wet (mid-range) models that exhibit strong positive future trends in temperature but little change in rainfall: HadGEM1, GFDL and CSIRO (green curves). These three models fall mid-range in terms of 20th century temperatures and rainfall. Their simulated 20th century rainfall is in closest agreement with CRU05 observations. All three models exhibit steep future warming trends (14–17%

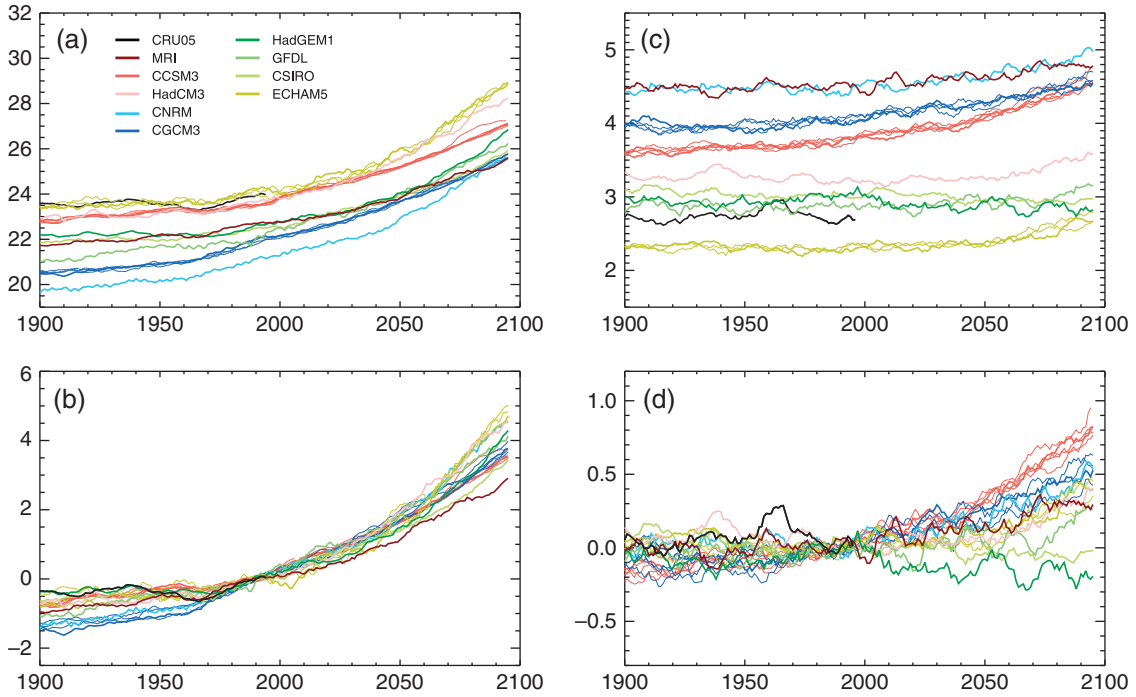

Fig. 1 Annual-average regional climate time series averaged for GCM land grid boxes within the East African region 12.5°N–12.5°S–25–42.5°E. Average values from the CRU05 baseline dataset are in black. Plotted are 10-year running mean values for 1900–2100 for (a) temperature (°C), (b) temperature anomalies w.r.t. the 1981–2000 period (°C), (c) precipitation (mm day^{-1}) and (d) precipitation anomalies w.r.t. the 1981–2000 period (mm day^{-1}). If there are a number of ensembles members for a GCM the first ensemble is plotted as solid lines and the remaining ensembles are plotted as thin solid lines.

Table 3 Annual-average surface temperature (°C) and rainfall (mm day^{-1}) averaged over the East African region: 12.5°N–12.5°S, 25°–42.5°E, for 1981–2000 and 2080–2099 and the absolute and percentage differences between (1980–1999)–(1981–2000) for CRU05 (1981–2000 only) and the GCMs

	Surface temperature (°C)				Precipitation (mm day^{-1})			
Climatology	1981–2000	2080–2099	Δ	%	1981–2000	2080–2099	Δ	%
CRU	23.9				2.7			
MRI	22.7	25.3	2.6	12	4.5	4.8	0.3	6
CCSM3	23.5	26.8	3.3	14	3.8	4.5	0.7	21
HADCM3	23.7	28.0	4.3	18	3.2	3.6	0.4	11
CNRM	21.1	25.3	4.2	20	4.4	4.9	0.5	10
CGCM3	22.0	25.5	3.5	16	4.0	4.5	0.5	12
HADGEM1	22.6	26.3	3.7	17	3.0	2.8	−0.2	−6
GFDL	22.1	25.9	3.8	17	2.9	3.1	0.2	7
CSIRO	22.5	25.6	3.1	14	3.0	2.9	−0.1	−1.5
ECHAM5	24.2	26.5	2.3	17	2.3	2.7	0.4	17
Mean	22.7	26.1			3.5	3.8		

GCMs are ordered in terms of their four groupings as discussed in 'Present-day and future climate projections' and 'Variation in ecosystem response among GCM types', where shading distinguishes the four GCM groups. Only the first ensemble member from the GCMs with multi-ensembles is shown.

increase in 2080–2099 w.r.t 1981–2000; Table 3). With regard to precipitation, GFDL displays an increase, CSIRO no trend and HadGEM1 a decrease over the 21st century.

Group 4: Warmest but driest model with strong positive future trend in temperature and rainfall: ECHAM5 (yellow curve). The three ECHAM5 ensembles project the hottest temperatures, in good agreement with CRU05

observations, but the lowest rainfall amounts over this region. They exhibit among the strongest positive future temperature and precipitation trends (17% increase in both temperature and rainfall in 2080–2099 w.r.t. present-day; Table 3).

Seasonal rainfall and soil moisture patterns are discussed in 'Future changes in seasonality among GCM groups'.

Results

Present-day biogeography and biogeochemistry

Under the CRU05 current climate (1981–2000), LPJ simulates rainforest or woodland dominated by evergreen trees (TrBE) in the warm, moist climate in the western part of the study area, comprising parts of DRC, Uganda and western Tanzania (Fig. 2). Drought-deciduous vegetation (woodland or savannah; TrBR) is predicted further north and south in slightly drier regions (annual precipitation, AP, $<4\,\mathrm{mm\,day^{-1}}$; Fig. 2b and d), while C_4 grassland (C4G) is predicted in the hottest and driest (AP $<2\,\mathrm{mm\,day^{-1}}$) parts of the study region to the east, comprising parts of Kenya and southern Ethiopia. The dominant PFT (Fig. 2d) shows a progression across the climate space of the region with TrBE in warm, wet areas shifting to TrBR in warm, moderately wet areas, C4G in the hottest, driest areas, and TE in the coolest parts of the region, reflecting the prescribed bioclimatic limits of the PFTs as shown in Table 1.

The PFT distributions are recategorised into characteristic biomes for East Africa, based on gridcell PFT and Leaf Area Index (LAI), following Hély *et al*. (2006) with some slight modifications (Fig. 2e). These were (a) that grid-cells with total LAI <2.0 and Woody LAI <4.5 were also classified as savanna types and (b) that steppe and desert grassland were defined for C4G coverage $\geq 10\%$ and $<10\%$, respectively. No grid-cells were defined uniquely as montane vegetation biomes since they also were categorised as forest or savanna biomes, hence this biome category was not included in Fig. 2e). Grid-cells dominated by woody PFTs correspond to forest and closed savanna biomes while grid-cells dominated by grassland vegetation correspond to open savanna and steppe and desert grassland biomes (Fig. 2d and e). The simulated biomes in Fig. 2e show broad-scale agreement with land cover classifications for natural vegetation for the region based on the MODIS/Terra (Friedl *et al*., 2002) and GLC2000 (JRL, 2005) satellite products for years 2001 and 2000, respectively (Fig. 3). In general, the evergreen, deciduous forest and closed savanna biomes derived from LPJ agree with the observed distribution of forest and woody savanna, while model-derived open savanna and steppe grassland biome distributions correspond to open savanna, shrubland and grassland in the satellite land cover classification. We also note that differences between biomes derived from model simulations of potential vegetation and satellite land-cover datasets may be in part related to human activities that are not included in LPJ, such as anthropogenic fires. The two satellite datasets showed good agreement among themselves in terms of natural vegetation coverage but differ markedly in the representation of croplands, as described in the 'Discussion'.

For the forest inventory data, vegetation carbon estimates from nine plots were compared with grid-cell results from the CRU05-driven simulation. The plot in the grid cell in the DRC (labelled 1 in Fig. 4) is in tropical moist forest dominated by evergreen tree species, and the model simulations are in good agreement to the plot estimates: 95% TrBE and 24.8 vs. 28.5 $\mathrm{kg\,C\,m^2}$. The comparison of this grid cell with LPJ outputs is the most robust as it is based on 46 ha of inventory data from a topographically relatively homogenous area. The plots in the two grid cells in Uganda also occur in tropical moist forest dominated by evergreen tree species. Simulated vegetation carbon in these two grid-cells are slightly lower compared with plot estimates (labelled 2–3 in Fig. 4), despite 95% TrBe coverage. The plots in the other three grid cells are in Tanzania within the Eastern Arc Mountain chain. They are all in closed canopy deciduous forest (low elevation plots) or submontane semi-deciduous forest (higher elevation plots). However, the landscape is complex, with grid cell areas likely to contain deciduous forest, dry woodland, bamboo, wooded grassland and grassland, depending on altitude. LPJ simulations reflect this complexity, with predictions from three grid squares of 79–89% TrBR, 1–3% TrBE and 7–19% C4G. However, carbon storage predictions were substantially lower than the plot estimates in two out of the three grid cells (labelled 5–6 in Fig. 4). The other three plots were located in grid cells simulated as dominated by C4G. Hence these three plots were not included in the regression below.

Reduced Major Axis regression (Fig. 4) shows that the forest inventory-based carbon storage estimates (x) are related to the CRU05-driven LPJ estimates for grid cells that predict forest (y) by

$$y = 1.04x - 8.40 (r^2 = 0.53; n = 6).$$

The slope coefficient is close to unity with a 95% CI that does not include zero (0.05–2.03), showing that the agreement is generally good. The intercept is negative, but the 95% CI spans zero (−37.5 to 20.7), and all but one of the six comparisons of LPJ forest-dominated predictions and inventory estimates were lower. This

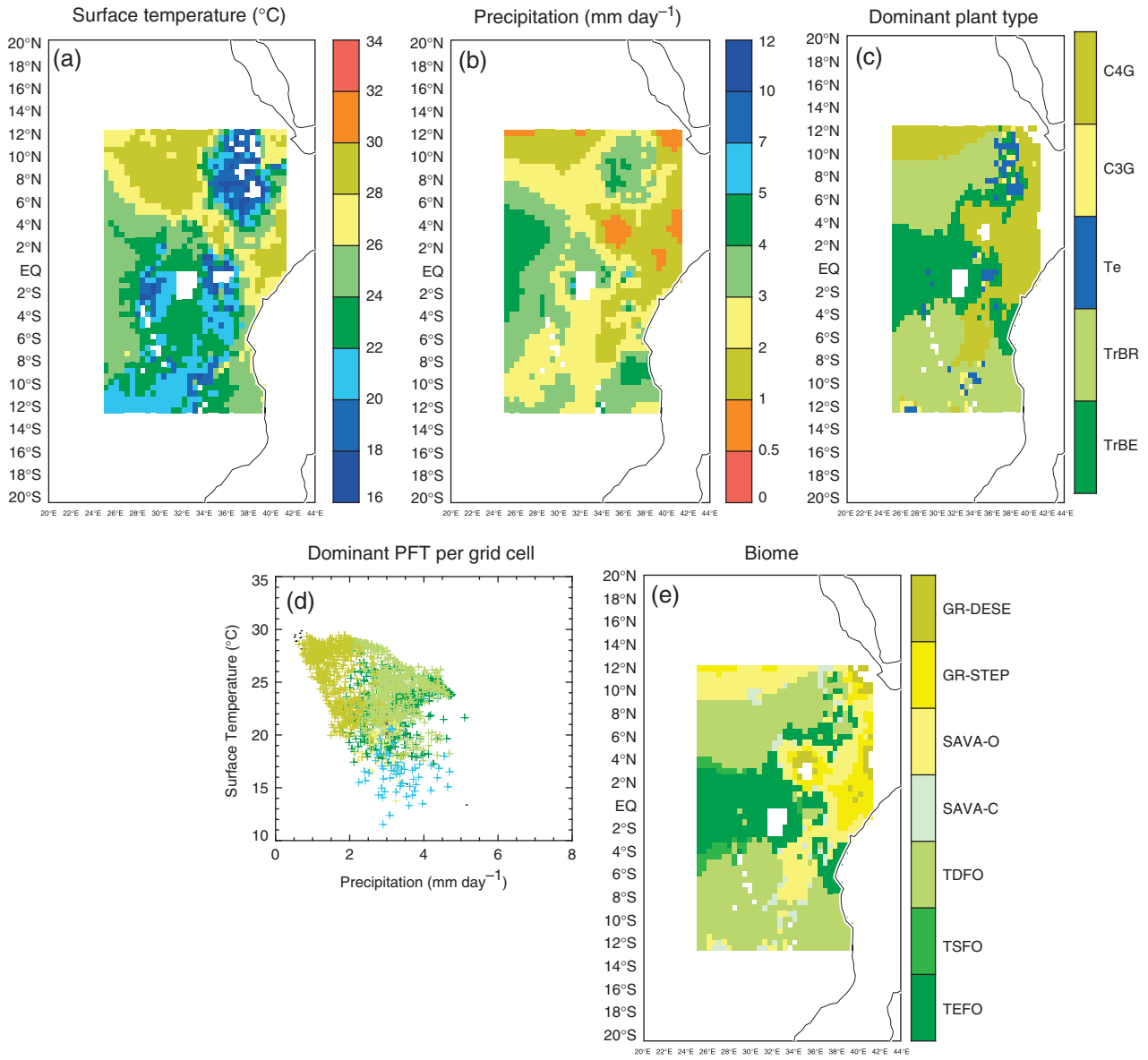

Fig. 2 Annual-mean CRU05 (a) Surface Temperature (°C), (b) Precipitation (mm day^{-1}) and (c) simulated LPJ-CRU05 Plant Functional Type: TrBE, TrBR, Te = TeBE, TeNE and TeBS, C3G and C4G; see Table 1, averaged over the present-day period 1981–2000, (d) plot of LPJ-CRU05 simulated dominant PFTs plotted in climate space, (e) Biomes derived from PFT and LAI distributions: TEFO, tropical evergreen forest; TSFO, tropical semi-deciduous forest; TDFO, tropical deciduous forest; SAVA-C, closed savanna, SAVA-O Open savanna; GR-STEP, grassland/steppe; GR-DESE, grassland/desert.

suggests that the LPJ model may be underestimating the carbon storage of East African forests.

If we assume this underestimation is linked to the predicted occurrence of grasses, which are absent from the forest inventory plots, then increasing the modelled vegetation C storage by the grassland coverage fraction would add only 0.7–2.1 kg C m^{-2} to these estimates, and would not substantially account for the underestimate (1.8–16.8 kg C m^{-2}) in 3 of the grid cells in the LPJ simulations. The differences may reflect both the limited inventory data and it whether it represents carbon storage at the grid cell scale or that the disjunct mountains are smaller than the grid cell size of CRU05 dataset and therefore the climate data is unrepresentative of the plot locations. Other causes may include model parameterisations or the tree allometry used or root : shoot ratio chosen, although forest plots in six grid cells is a very small sample size from which to draw firm conclusions.

The spatial patterns of dominant plant types in the GCM-driven simulations averaged over 1981–2000

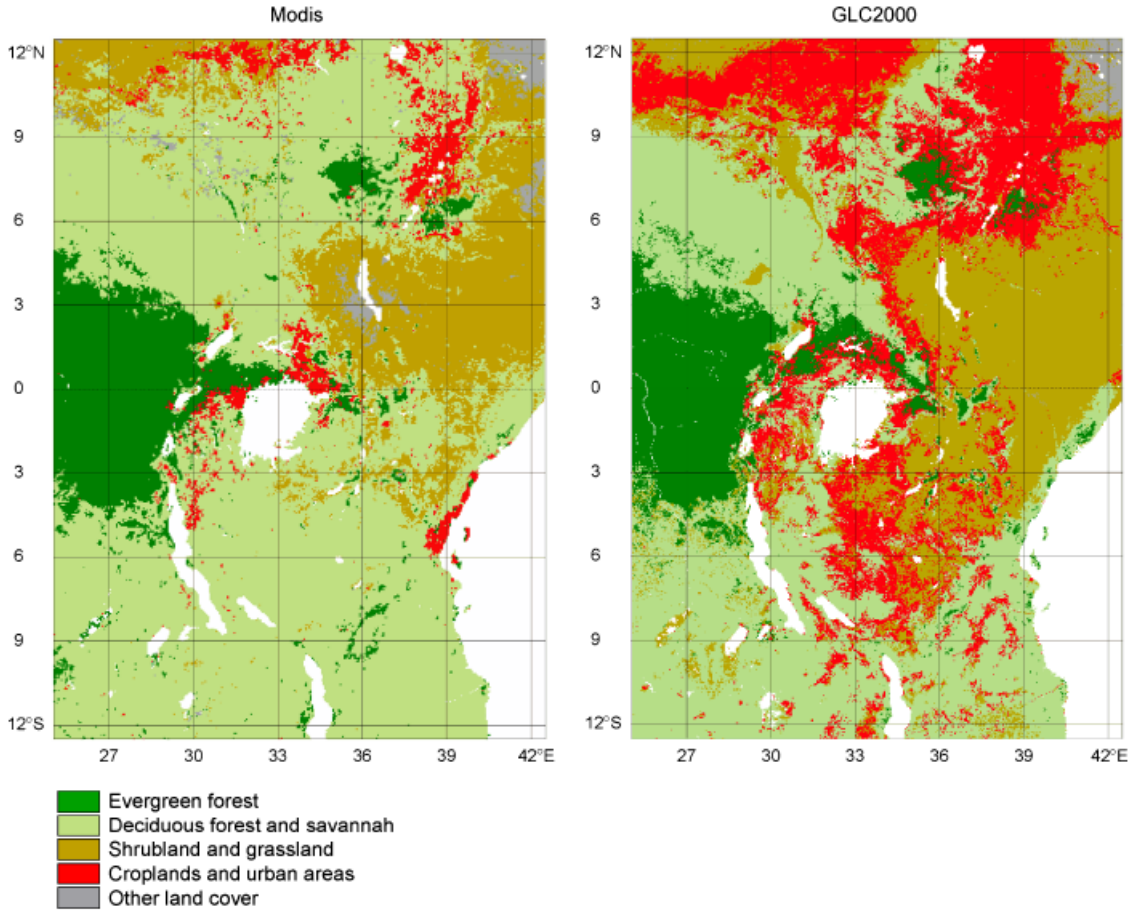

Fig. 3 Land-cover over the East African study region according to the MODIS/Terra global 0.05 degree land cover classification for 2001 (Friedl *et al*., 2002), and GLC 2000 (JRL, 2005). The original 17 classes of the 'Type 1' (IGBP) land cover legend have been reduced to five aggregate classes for optimal comparison with the vegetation model output from this study (see text). MODIS source: NASA-EOS Data Gateway, http://wist.echo.nasa.gov; page visited 11 August 2008.

generally show fair agreement with those derived using the CRU05 climate. Consequences of different GCM grid resolutions for the projected vegetation patterns are illustrated in Fig. 5. Spatial patterns of dominant PFTS derived from LPJ simulations using climate projections from some of the higher resolution models CSIRO, ECHAM5, GFDL and HadGEM1 (Fig. 5) give the closest agreement. Some of the wetter models (e.g. CNRM) suggest temperate tree coverage not reproduced by LPJ for the CRU05 climate. The percentage coverage of each PFT averaged over the region over the 20th century depicts similar results (Fig. 6). Individual model biases are discussed in more detail in 'Variation in ecosystem response among GCM types'.

Regional-average NPP, R_h and total ecosystem carbon stocks were projected to increase over the 20th century (Fig. 7), suggestive of a plant physiological response to the observed rise in CO_2 over this period ('Driving climate, atmospheric CO_2 concentrations and soils' and 'Discussion'). A pronounced carbon cycle response to the anomalously high rainfall during the 1960s (Fig. 1) is also evident, with greater soil moisture during this period (not shown) leading to higher NPP and R_h as well as vegetation, soil and total ecosystem carbon pools, but lower wildfire emissions (C_{fire}) (Fig. 7). The majority of GCM-driven simulations result in higher NPP (Table 4) and R_h over the 20th century than is simulated under CRU05 climate. The simulations driven by climate from CSIRO, CGCM3 and GFDL yield the closest agreement to the CRU05-driven simulation in terms of NPP and R_h (Table 4). Simulated total ecosystem carbon is also higher in the GCM (apart from ECHAM5)-driven simulations compared with the CRU05-driven simulation (Table 4). Equilibrium values for vegetation and soil carbon pools at the start of the simulations (year 1850–1860 depending on GCM) ranged between 8.5–23.2 and 7.6–10.1 kg C m^{-2}, similar to the present-day values in Table 4.

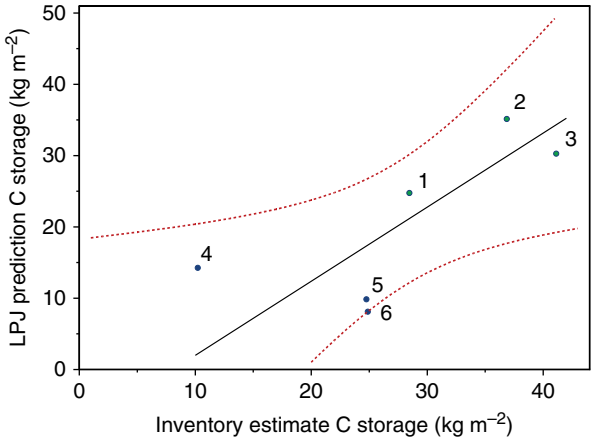

Fig. 4 Carbon stock estimates from forest inventory plots grouped into 0.5×0.5 degree grid cells plotted against CRU05 driven LPJ predictions of carbon stocks, and reduced major axis regression line fitted (black line and equation in text). Plots in the DRC (1) and Uganda (2–3) are coloured in green and labelled (1–3), while the plots in Tanzania are coloured in blue (labelled 4–6). LPJ predictions were for the same year as the inventory data if the inventory data was before 2002, for post-2002 inventory data (5–6) LPJ predictions for 2002 were used. The 95% confidence interval (CI) on the slope is plotted in red.

Future projections of biogeography and biogeochemistry

In the latter part of the 21st century, TrBE and TrBr coverage increase at the expense of C4G in all LPJ simulations, regardless of GCM (Fig. 6). Model simulations that depict some temperate trees and C3G for the present-day show rapid decline in their fractional coverages in the future.

Despite overall increases in woody coverage, no major shifts in dominant PFTs over the region are projected for the future (Fig. 8). Some minor shifts are apparent by 2080–2099 over small parts of eastern and coastal East Africa ($\sim 38^{\circ}$E), the most consistent pattern being a replacement of C4G by TrBE in several grid-cells in the northern-hemisphere part of the domain and by TrBR in some southern parts of the domain in a number of simulations (Fig. 8).

Strong positive future trends in NPP are projected independent of GCM with NPP increasing by 153–314 g C m^{-2} yr^{-1} (Fig. 7a, 18–36%; Table 4) by 2080–2099 w.r.t. present-day. All simulations suggest a strong positive future trend in R_h (Fig. 7b). Wildfire emissions increase by 3–59 g C m^{-2} yr^{-1} in 2080–2099 compared with present-day (Fig. 7c, Table 4). The net ecosystem exchange (NEE) is a residual term given by

$$\mathrm{NEE} = \mathrm{R_h} - \mathrm{NPP} + \mathrm{C_{fire}}.$$

Here, a positive NEE represents a source of CO_2 to the atmosphere. Eight out of nine simulations show a present-day carbon sink over East Africa, and the mean sink is projected to increase slightly ($\sim 17\%$) in 2080–2099 compared with present-day (Fig. 7d, Table 4). Only two GCMs (ECHAM5 and HADGEM1) were associated with an annual net carbon source to the atmosphere in the final decades of the 21st century. Interdecadal variations are considerable in all simulations (Fig. 7d).

Regional-average vegetation carbon increases in all future simulations, reflecting NPP trends. By 2080–2099, vegetation carbon increases by 1.2–3.3 kg C m^{-2} (Fig. 7e; 9–22%; Table 4) compared with present-day. Soil carbon anomalies in most GCM-driven simulations display either a small increase or little change followed by a decrease after 2050–2070. This small decreasing trend in soil carbon in the majority of the simulations (Fig. 7f; $+1$ to -8%; Table 4), is dominated by the increase in R_h, primarily in response to soil warming. Total carbon storage is generally dominated by the vegetation carbon response (Fig. 7g) with increases of 0.6–3.3 kg C m^{-2} (3–13%; Table 4) by 2080–2099.

Future reductions in regional actual evapo-transpiration (AET) were simulated under all GCM climates despite increased precipitation (Table 5). Increased temperatures lead to increased evaporative demand for water vapour, resulting in protective stomatal closure. LPJ also simulates increased plant water-use efficiency and reduced stomatal aperture under elevated CO_2. Decreases in AET combined with increased future precipitation explain the projected increases in runoff and soil moisture content seen in most simulations (Table 5).

Variation in ecosystem response among GCM types

Group 1: Warmer, wetter models that generally exhibit strong positive future trends in temperature as well as positive future trends in rainfall: MRI, CCSM3 and HadCM3. The warmer wetter regional climate simulated by these three models over the 20th century is favourable for tropical evergreen forest according to LPJ. Simulations driven by these GCMs yield the highest fractional coverage of TrBE under the present climate (Fig. 6), extending further east compared with the CRU05-driven simulation, reflecting the wet bias in these models (Figs 1 and 2). Moderate increases (highest in CCSM3) of TrBE are simulated for the future. Relatively high fractional coverage of TrBR is also simulated, with future increases (Fig. 6). The CCSM3 and HadCM3-driven simulations yield high C4G coverage in the 20th century that declines in the future as the climate wettens (Figs 1 and 9).

The warm, wet climates produce the highest simulated NPP (Table 4) and R_h for 1981–2000. The combination of high baseline values and strong positive future trends in NPP and R_h as the climate

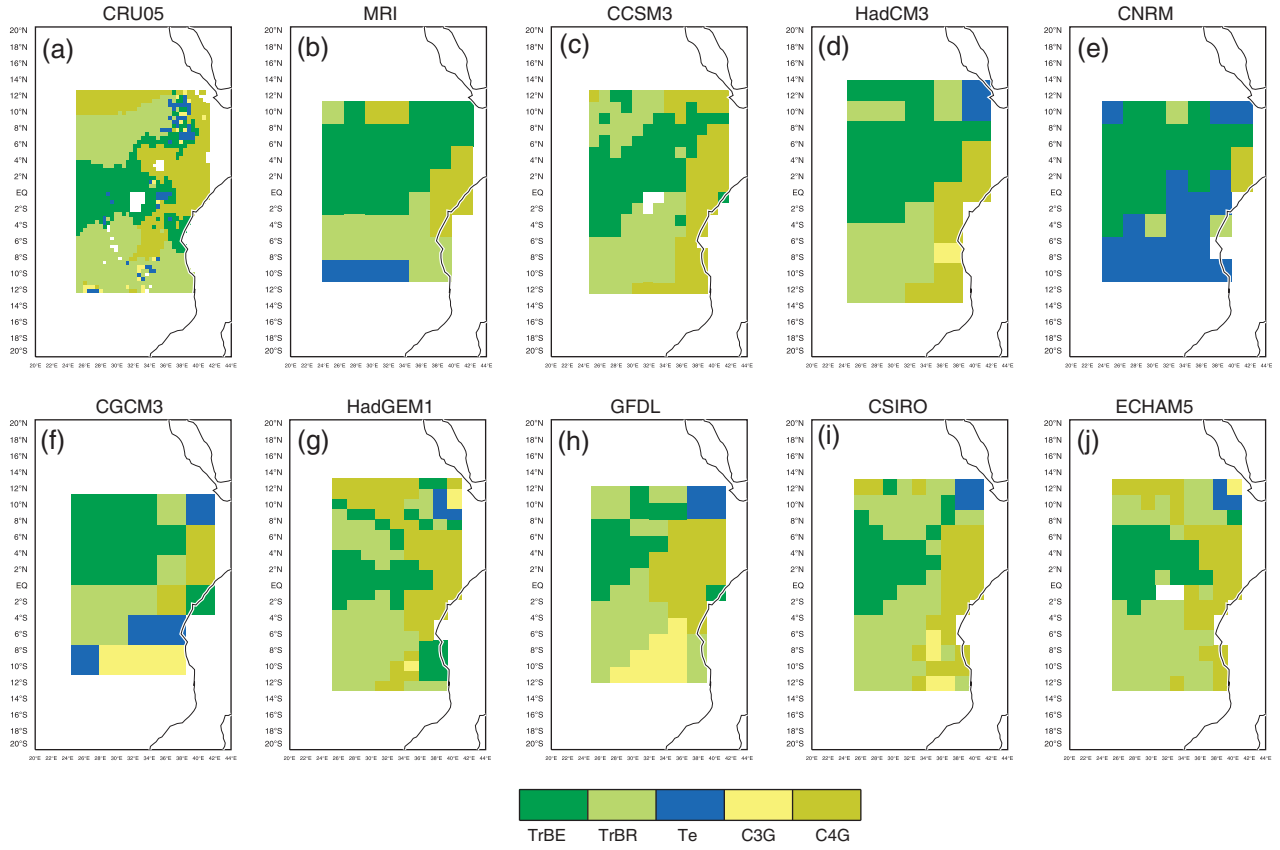

Fig. 5 Spatial patterns of the dominant plant functional type (PFT) predicted by LPJ for the 1981–2000 driven by (a) the CRU05 observed climate dataset and (b–j) the nine GCM-driven simulations. Note only the first ensemble member from the GCMs with multi-ensembles is shown. Dominant plant type is derived from decadal-mean annual average fractional cover of PFTs: TrBE, TrBR, Te = TeBE, TeNE and TeBS, C3G and C4G; see Table 1.

becomes warmer and wetter results in the largest simulated NPP and R_h by 2080–2099 (Fig. 7a and b, Table 4). Wildfire emission trends are positive due to greater fuel loads from higher litter production (see 'Future changes in seasonally among GCM groups'). NEE maintains a trend towards increasing carbon sinks in the future in two of the simulations, while the MRI climate is associated with a slight decrease. These simulations also yield the largest biomass carbon pools (Table 4). The large increases in NPP and woody coverage (largest for CCSM3) result in a positive future trend in vegetation carbon. The encroachment of trees onto grassland areas in the CCSM3-driven simulations amplifies the strong positive vegetation carbon trend. NPP increases propogate (via litter input) to relatively high soil carbon pools, which increase (MRI) or decrease (CCSM3, HadCM3) slightly in the future depending on the net influence of the warmer, wetter future climate on NPP and R_h. Total carbon storage largely reflects vegetation carbon pools (Fig. 7g). The projected ecosystem carbon storage for 2080–2099 is highest in the simulations driven by these three GCMs (Table 4). The CCSM3 and HADCM3 driven simulations suggest large increases in runoff and soil moisture content (Table 5).

Group 2: Cooler, wetter models that exhibit strong positive future trends in temperature and rainfall: CNRM and CGCM3. Despite lower temperatures, the moist climates favour TrBE and TrBR, with increases in these PFTs under the future warming (Figs 6 and 9). The TrBE range is shifted north under the present climate compared with the CRU05-driven simulation, due to a wet bias in this area. Temperate trees are simulated in southern areas (Figs 5, 6 and 9) due to a present-day cold bias (Fig. 1); these decline rapidly in the warming future climate.

Extant NPP and R_h are relatively low in these simulations but exhibit strong positive trends as the climate warms (30–36% increase in NPP in 2080–2099 compared with present-day; Table 4). NPP values in 2080–2099 are the second largest after the Group 1

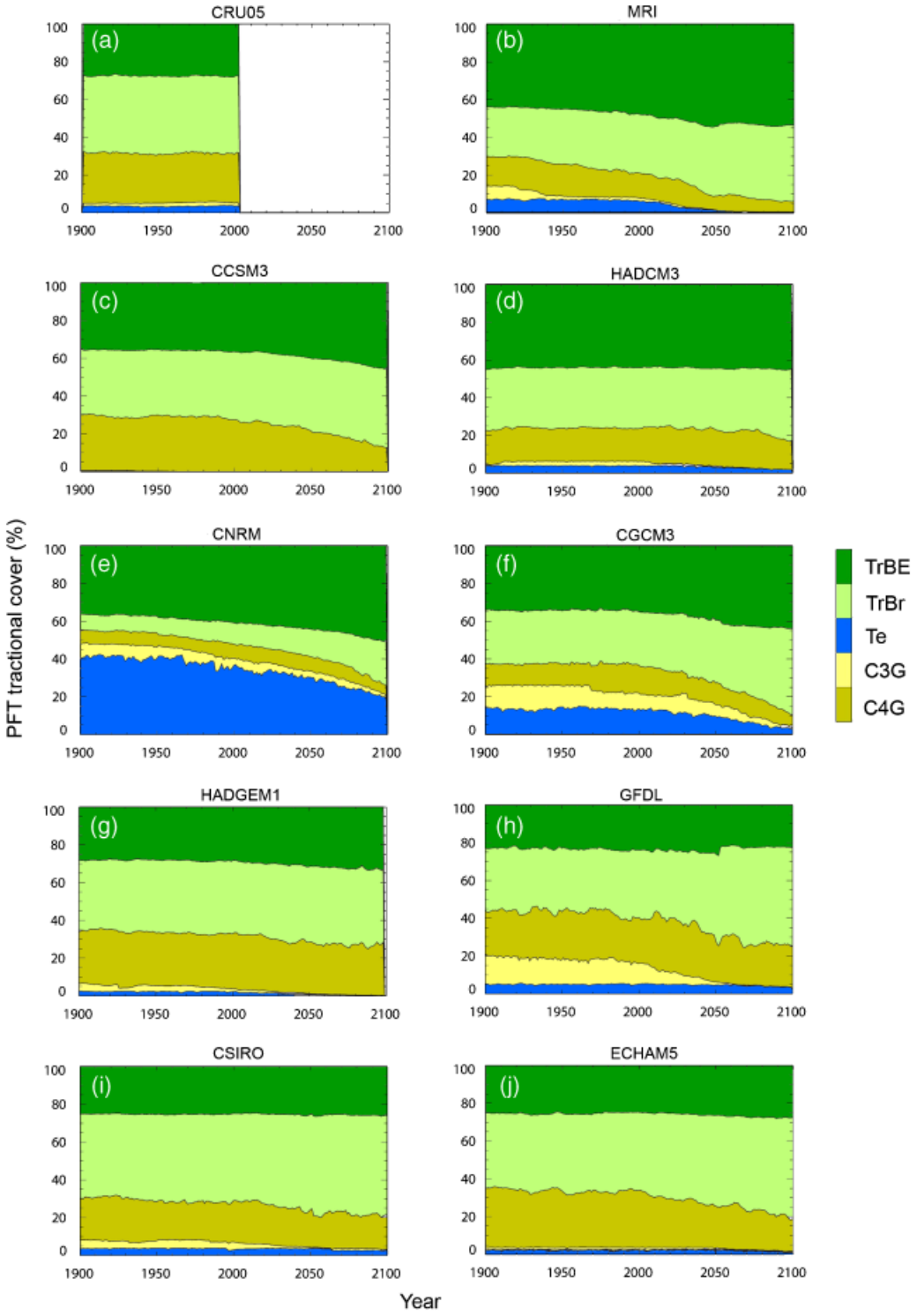

Fig. 6 Simulated temporal changes in fractional coverage of plant functional types (PFTs): TrBE, TrBR, Te = TeBE, TeNE and TeBS, C3G and C4G; see Table 1, for 1900–2100 averaged over the East African study region 12.5°N–12.5°S–25–42.5°E.

GCMs (Table 4). C_{fire} exhibits a slight positive future trend, the wetter climate offsetting somewhat the positive effect of higher litter input. CGCM3 is the only model that suggests a present-day carbon source, albeit a small one (Table 4). Carbon sinks are simulated under the future climate for both GCMs (Fig. 7d). Present-day vegetation carbon estimates lie mid-range (Table 4), and increase moderately in the future (Fig. 7e).

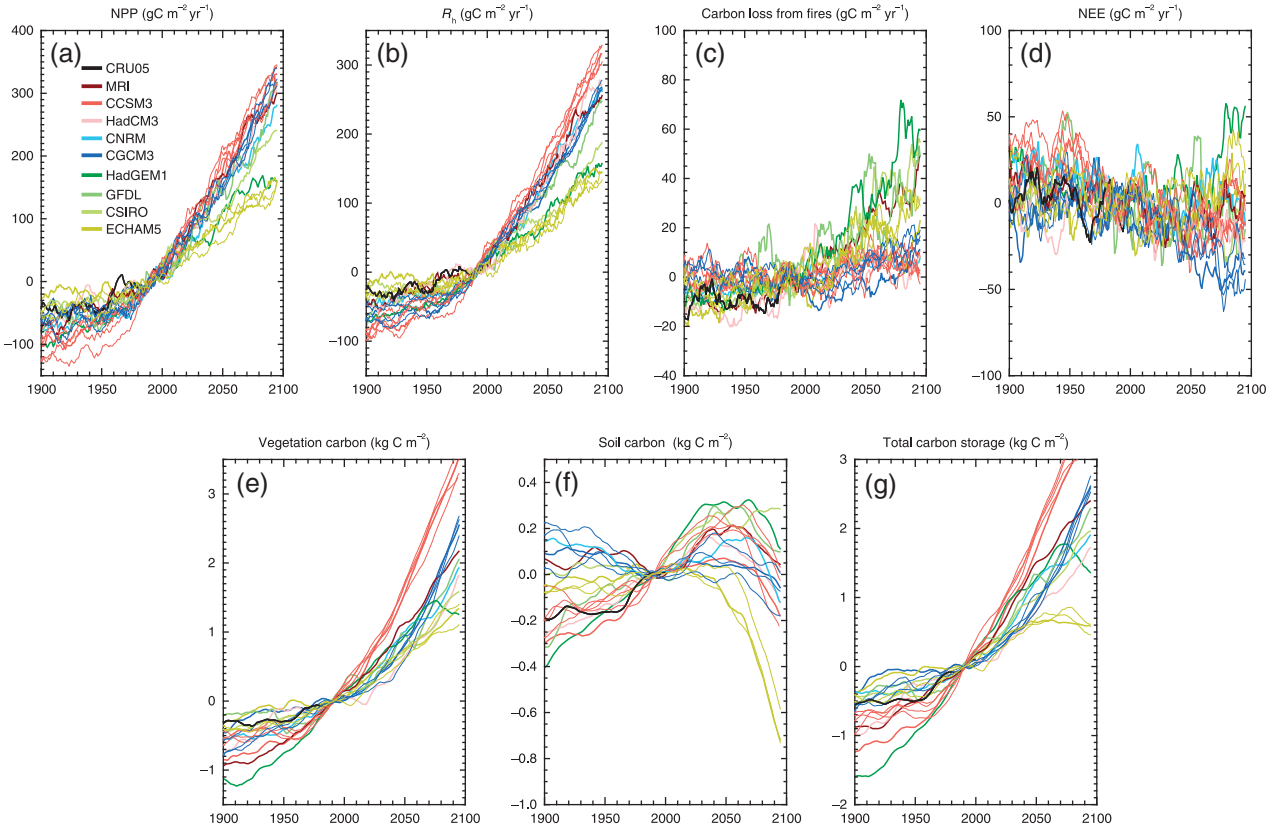

Fig. 7 Annual-average regional time series of carbon fluxes averaged for GCM land grid boxes within the East African region 12.5°N–12.5°S–25–42.5°E. Average values from the CRU05-derived LPJ simulation are in black. Plotted are 10-year running mean values for 1900–2100 for (a) NPP anomalies, (b) heterotropic respiration (Rh) anomalies, (c) carbon loss due to fires (C_{fire}) anomalies, (d) net ecosystem exchange (NEE = R_h-NPP + C_{fire}) anomalies, (e) vegetation carbon anomalies, (f) soil carbon anomalies, (g) total carbon (sum of litter, vegetation and soil carbon pools) anomalies, all w.r.t. the 1981–2000 period. Units for (a–d) are g C m^{-2} yr^{-1} and for (e–g) are kg C m^{-2}. If there are a number of ensembles members for a GCM the first ensemble is plotted as solid lines and the remaining ensembles plotted as thin solid lines.

Soil carbon pools show little change in the future. Total projected carbon storage in 2080–2099 is the second largest after the Group 1-based simulations (Table 4, Fig. 7g). After CCSM3 and along with ECHAM5, these models are associated with the greatest (in absolute terms) future increases in runoff, moderate-large increases in soil moisture content and the largest decreases in AET (apart from MRI) (Table 5).

Group 3: Fairly warm and dry (mid-range) models that exhibit strong positive future trends in temperature but little change in rainfall: HadGEM1, GFDL and CSIRO. The warmer and relatively dry climates predicted by these GCMs give rise to lower present-day TrBE fractional coverage compared with the other simulations apart from ECHAM5 (Fig. 6). Future trends are only slightly positive for TrBE. The climate is generally more favourable for C4G and TrBR – the latter increases in the future. Temperate (C3G) grasses are also simulated in these simulations but decline rapidly in the future (Figs 6 and 9).

NPP and R_h under the CSIRO and GFDL present-day (1981–2000) climate are at the lower end of the projected ranges (Table 4), but give the closest agreement to results from the CRU05 simulations. The HadGEM1-driven simulation yields larger NPP and R_h values for present-day comparable to results from Group 2 GCM simulations. Future trends in NPP and R_h are strongly positive for GFDL and CSIRO but relatively small for HadGEM1 (Fig. 7a and b), although 2080–2099 values remain at the lower end of model projections. Wildfire emissions increase in the future as warmer temperatures and higher evapotranspiration combined with little change (GFDL) or small future decreases in precipitation (CSIRO, HadGEM1; Table 2) lead to drier fuel loads (see 'Future changes in seasonally among GCM groups'). Carbon sinks increase in the future, except in the HadGEM1-driven simulation where the

Table 4 LPJ-simulated annual mean net primary production (NPP), wildfire carbon emissions (C_{fire}), net ecosystem exchange (NEE = R_h−NPP + C_{fire}) ($g\,C\,m^{-2}\,yr^{-1}$) and vegetation, soil and total carbon pools (vegetation, litter & soil) ($kg\,C\,m^{-2}$) averaged over the East African study region for the periods 1981–2000 and 2080–2099 and the absolute and percentages change between them

	NPP ($g\,C\,m^{-2}\,yr^{-1}$)				C_{fire} ($g\,C\,m^{-2}\,yr^{-1}$)				NEE ($g\,C\,m^{-2}\,yr^{-1}$)		
Climatology	1981–2000	2080–2099	Δ	%	1981–2000	2080–2099	Δ	%	1981–2000	2080–2099	%
CRU	771.7				105.6				−9.5		
MRI	1174.2	1457.2	282.9	24	116.7	156.5	39.8	34	−18.3	−17.0	↑
CCSM3	1013.1	1327.5	314.3	31	102.2	105.6	3.4	3	−20.6	−34.8	↓ *
HADCM3	1004.2	1297.0	292.8	28	113.1	116.9	3.8	3	−8.0	−26.6	↓
CNRM	861.9	1120.7	258.7	30	83.3	90.1	6.8	8	−21.5	−25.3	↓
CGCM3	818.8	1114.9	296.0	36	97.2	105.2	8.0	8	2.0	−38.4	↓ *
HADGEM1	880.3	1042.2	161.8	18	103.1	162.5	59.4	58	−26.8	+ 21.5	↑
GFDL	800.6	1085.7	285.1	36	99.1	140.6	41.5	42	−19.3	−33.8	↓
CSIRO	821.0	1051.0	230.0	28	114.9	159.2	44.3	39	−9.2	−21.8	↓
ECHAM5	710.1	863.4	153.3	22	98.0	110.3	12.3	13	−1.0	+ 2.8	↑ *
GCM mean	898.2	1151.1			103.1	127.4			−13.6	−19.3	

	Vegetation carbon ($kg\,C\,m^{-2}$)				Soil carbon ($kg\,C\,m^{-2}$)				Total carbon stocks ($kg\,C\,m^{-2}$)			
Climatology	1981–2000	2080–2099	Δ	%	1981–2000	2080–2099	Δ	%	1981–2000	2080–2099	Δ	%
CRU	10.4				8.1				19.3			
MRI	23.8	25.8	2.0	9	10.2	10.3	0.1	1	35.2	37.5	2.3	7
CCSM3	14.9	18.2	3.3	22	9.3	9.2	−0.1	−1	25.2	28.5	3.3	13
HADCM3	16.7	18.4	1.6	10	8.7	8.6	−0.1	−1	26.4	28.0	1.6	6
CNRM	14.2	15.9	1.8	12	7.7	7.6	−0.05	−1	22.7	24.5	1.8	8
CGCM3	13.2	15.5	2.3	18	8.1	8.1	−0.03	−0	22.2	24.6	2.4	11
HADGEM1	12.4	13.7	1.3	10	9.1	9.3	0.2	2	22.4	24.0	1.5	6
GFDL	10.2	12.1	1.8	18	8.9	9.0	0.2	1	20.0	22.0	2.0	10
CSIRO	13.2	14.7	1.5	11	8.2	8.5	0.3	3	22.3	24.2	1.9	8
ECHAM5	9.0	10.2	1.2	14	7.7	7.1	−0.6	−8	17.4	18.0	0.6	3
GCM mean	14.2	16.1			8.7	8.6			23.8	25.7		

*Of five CCSM3 ensembles, three ensembles exhibit a ↓ trend, one ensemble exhibits no trend and one ensemble exhibits an upward trend. All four CGCM3 ensembles exhibit a ↓ trend, while all three ECHAM5 ensembles show a ↑ trend.

Results are from simulations driven by CRU05 observed climate (1981–2000) and the nine GCMs (Table 3). GCMs are ordered in terms of their four groupings as discussed in 'Present-day and future climate projections' and 'Variation in ecosystem response among GCM types', where shading distinguishes the four GCM groups. Results based on the first ensemble member only from the GCMs with multi-ensembles are shown.

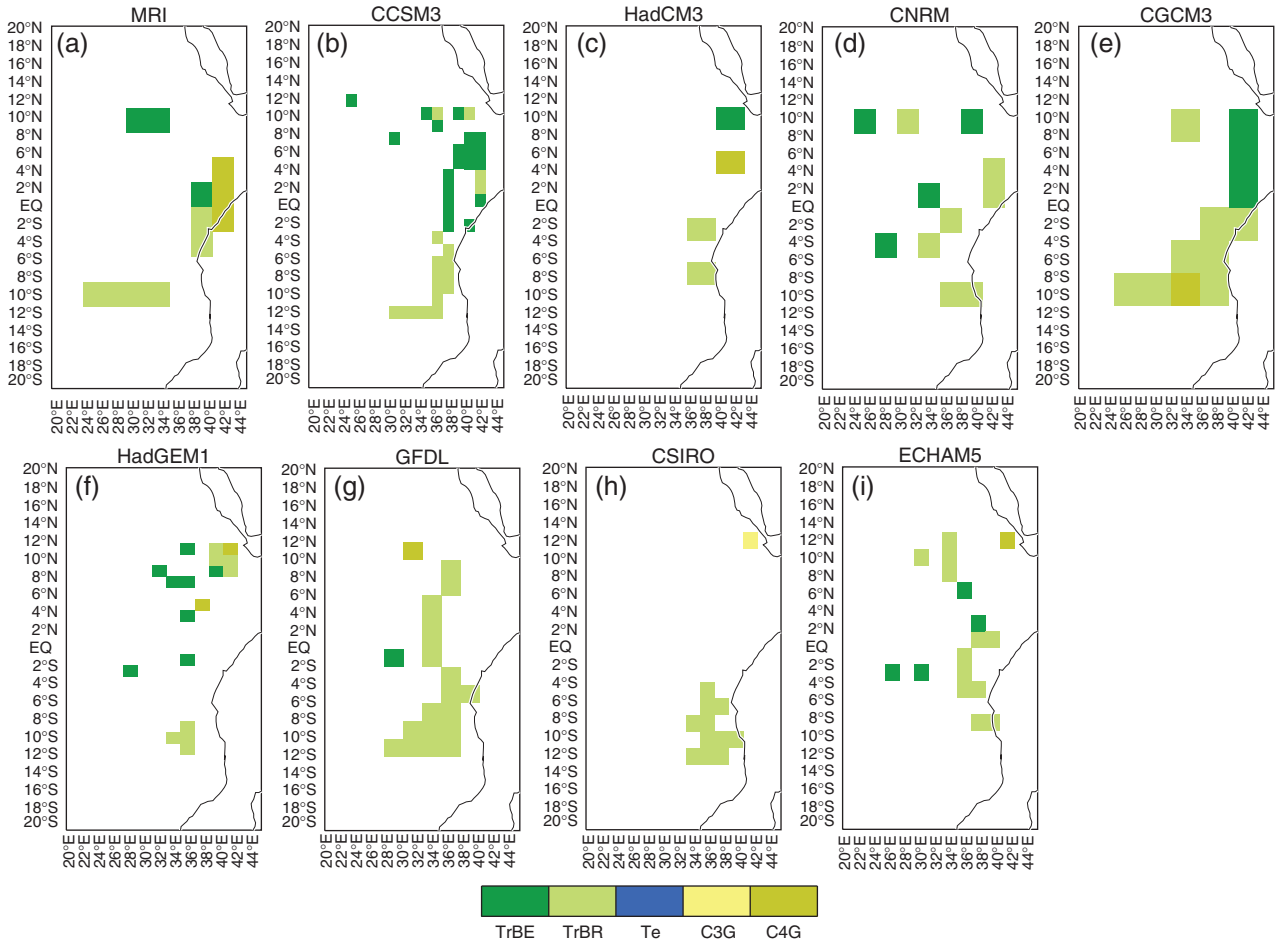

Fig. 8 Spatial patterns that depict grid-cells where a transition in dominant plant functional type (PFT) between the 2080–2099 and 1981–2000 occurs. Plotted are the dominant PFTs averaged over the period 2080–2099 for the nine GCM-driven simulations. Note only the first ensemble member from the GCMs with multi-ensembles is shown. Dominant plant type is derived from annual average fractional cover of individual PFTs (TrBE, TrBR, Te = TeBE, TeNE and TeBS, C3G and C4G; Table 1).

strong positive C_{fire} trend leads to an overall positive trend in NEE that becomes a carbon source by the end of the 21st century (Fig. 7d). Vegetation carbon pools are smaller for this group of simulations compared with Groups 1 and 2 (Table 4), due mainly to the low coverage of trees. Future changes are also small (Fig. 7e). Soil carbon shows small future increases (Fig. 7b). Projected total carbon storage in 2080–2099 is only slightly lower compared with simulations driven by the Group 2 GCMs (Table 4). In the future, simulated runoff increases are among the lowest for GFDL and CSIRO, while the decrease in precipitation in HadGEM1 leads to decreased runoff and soil moisture content.

Group 4: Warmer but drier model with strong positive future trends in temperature and rainfall: ECHAM5. The warm temperatures and drier climate gives similar regional vegetation coverage to that simulated by the Group 3 GCMs with a dominance of TrBR, which shows an increase towards the end of the 21st century (Fig. 6).

The warm, dry climate results in among the lowest NPP and R_h under present-day conditions, with moderate increases in the future. By 2080–2099, NPP is the lowest among all simulations (Table 4). The climate from all three ECHAM5 ensemble members results in a small positive NEE trend and a regional carbon source in the future (Fig. 7d, Table 4). Relatively low vegetation carbon results from a combination of low NPP and moderately low tree coverage. Future vegetation carbon in 2080–2099 is the smallest compared with the other three groups of GCMs (Table 4). Soil carbon stocks are also the lowest, due to low productivity during the 20th century, and ECHAM5 simulates the largest decline in soil carbon in the future as R_h increases. Total carbon storage reflects

Table 5 LPJ-simulated annual mean runoff, actual evapotranspiration (AET), annual fraction of grid cell burnt and soil moisture content averaged over the East African study region for the periods 1981–2000 and 2080–2099 and the absolute and percentage changes between them

	Runoff (mm yr^{-1})				AET (mm yr^{-1})				Soil moisture content (fraction)				Fraction of grid-cell burnt (/year)			
Climatology	1981–2000	2080–2099	Δ	%	1981–2000	2080–2099	Δ	%	1981–2000	2080–2099	Δ	%	1981–2000	2080–2099	Δ	%
CRU	234.5				521.0				0.39				0.030			
MRI	637.9	714.3	76.4	12	700.0	594.1	−105.9	−15	0.56	0.57	0.01	3	0.010	0.012	0.002	23
CCSM3	468.7	680.3	211.6	45	645.7	589.7	−56.0	−9	0.50	0.57	0.07	14	0.023	0.017	−0.006	−28
HADCM3	421.3	508.6	87.2	21	675.6	660.4	−15.2	−2	0.49	0.53	0.03	6	0.019	0.021	0.002	7
CNRM	752.9	891.2	138.4	18	667.4	584.7	−82.6	−12	0.59	0.61	0.02	3	0.011	0.010	−0.002	−14
CGCM3	752.7	905.6	153.0	20	548.4	485.8	−62.6	−11	0.56	0.60	0.04	8	0.016	0.017	0.001	9
HADGEM1	366.9	333.7	−33.2	−9	558.7	528.7	−30.0	−5	0.42	0.39	−0.03	−7	0.020	0.035	0.015	72
GFDL	419.2	460.1	40.8	10	540.7	506.1	−34.6	−6	0.47	0.48	0.01	3	0.039	0.043	0.004	11
CSIRO	413.7	416.5	2.8	1	530.2	482.2	−48.0	−9	0.48	0.47	−0.01	−2	0.029	0.033	0.003	11
ECHAM5	284.3	425.2	140.9	50	488.4	444.4	−43.9	−9	0.42	0.49	0.07	16	0.034	0.031	−0.003	−8
GCM Mean	502.0	595.9			595.0	541.8			0.50	0.52			0.022	0.024		

Soil moisture content is expressed as a fraction over the 1.5 m LPJ soil column. Results are from simulations driven by CRU05 observed climate (1981–2000) and the nine GCMs (Table 3). GCMs are ordered in terms of their four groupings as discussed in Sections 'Present-day and future climate projections' and 'Variation in ecosystem response among GCM types', where shading distinguishes the four GCM groups. Results based on the first ensemble member only from the GCMs with multi-ensembles are shown.

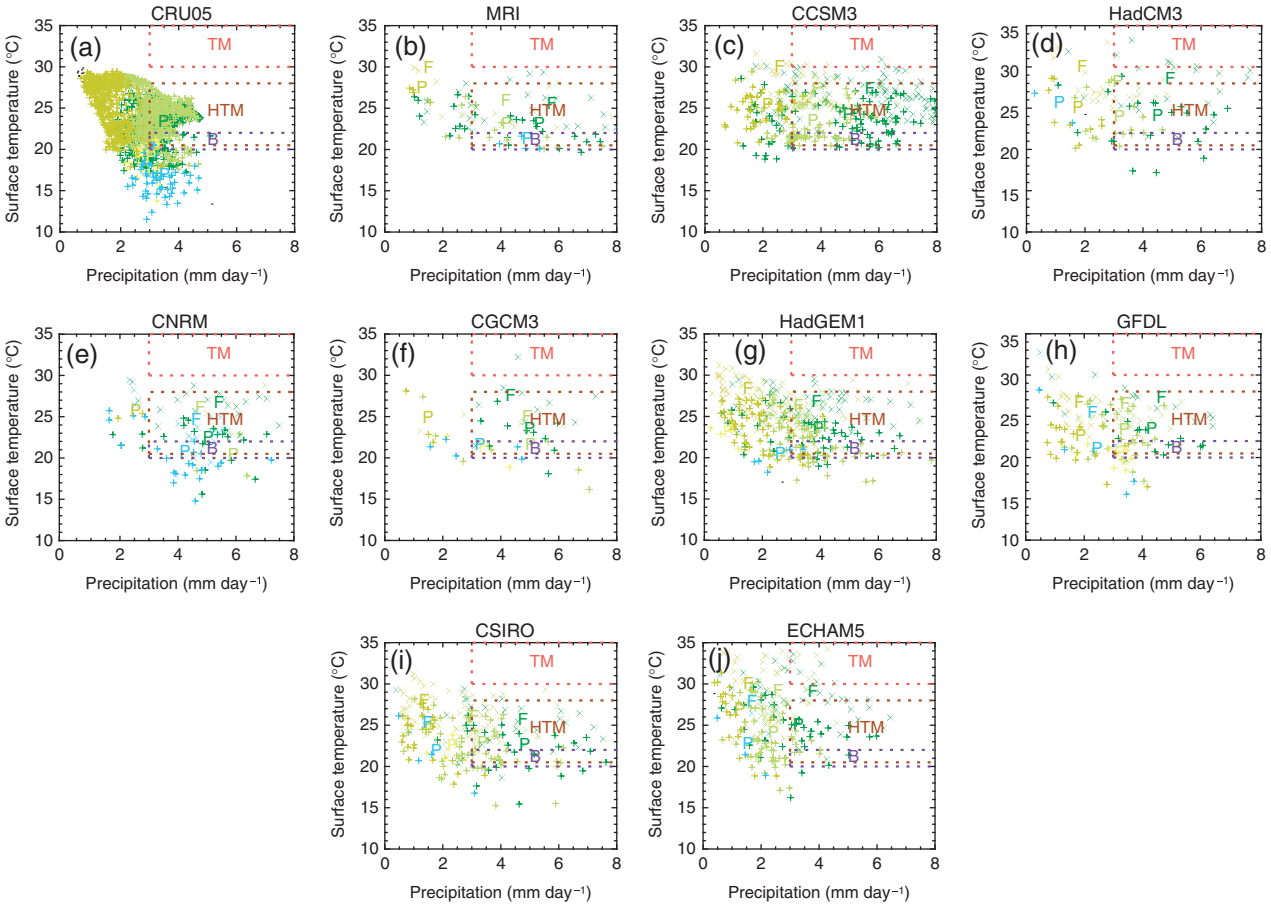

Fig. 9 Simulated dominant plant functional types for each East African grid-cell plotted in climate space (annual average precipitation vs. annual average temperature) for the CRU05 and nine GCM simulations for 1981–2000 (+) and 2090–2099 (×). 'P' and 'F' represent the average climate limits for each PFT across all the grid-cells for 1981–2000 and 2080–2099, respectively. Optimum average temperature and precipitation ranges for tropical maize (TM), tropical highland maize (HTM) and beans (B) are overlaid for comparison. Note that these crop ranges do not account for increasing water demand with increasing temperatures.

both the vegetation and soil carbon trends, and is the lowest among all simulations in 2080–2099 (Table 4). Future runoff and soil moisture increases are largest in percentage terms (Table 5).

Future changes in seasonality among GCM groups

The East African region covers areas with unimodal and bimodal annual rainfall patterns, with bimodal patterns restricted to equatorial latitudes between about 3°N and 3°S (Jones & Thornton, 2001). Wet seasons occur around October–December (long rains) and March–May (short rains) with a dry season between June and August. Further north of the equator there tends to be one distinct wet season and a dry season that runs from February to April. South of 3°S the climate again becomes unimodal with a dry season occurring between August and October (Jones & Thornton, 2001). The patterns of rainfall seasonality averaged over the region (not shown) are accurately reflected in the simulated moisture content for the top 50 cm of the soil (layer 1; Fig. 10). Seasonal cycles from the CRU05 dataset show the distinct unimodal and bimodal seasons discussed above and the effect of averaging over the region (Fig. 10a). The amplitude of annual-average soil moisture is higher in forest-dominated regions (between 0.42 and 0.47) than in regions dominated by grasses (0.21), with the exception of the few high-altitude grid cells simulated as C3G by the model (not shown). The seasonality of soil moisture does not appear to have an overriding influence on the simulated dominant PFT.

All the GCMs simulate a stronger seasonal cycle over 1981–2000 than CRU05 and a driest period between May/June and July/August. Rainfall/soil moisture patterns shows little change in the future (Fig. 10). Generally the wet seasons become wetter (by up

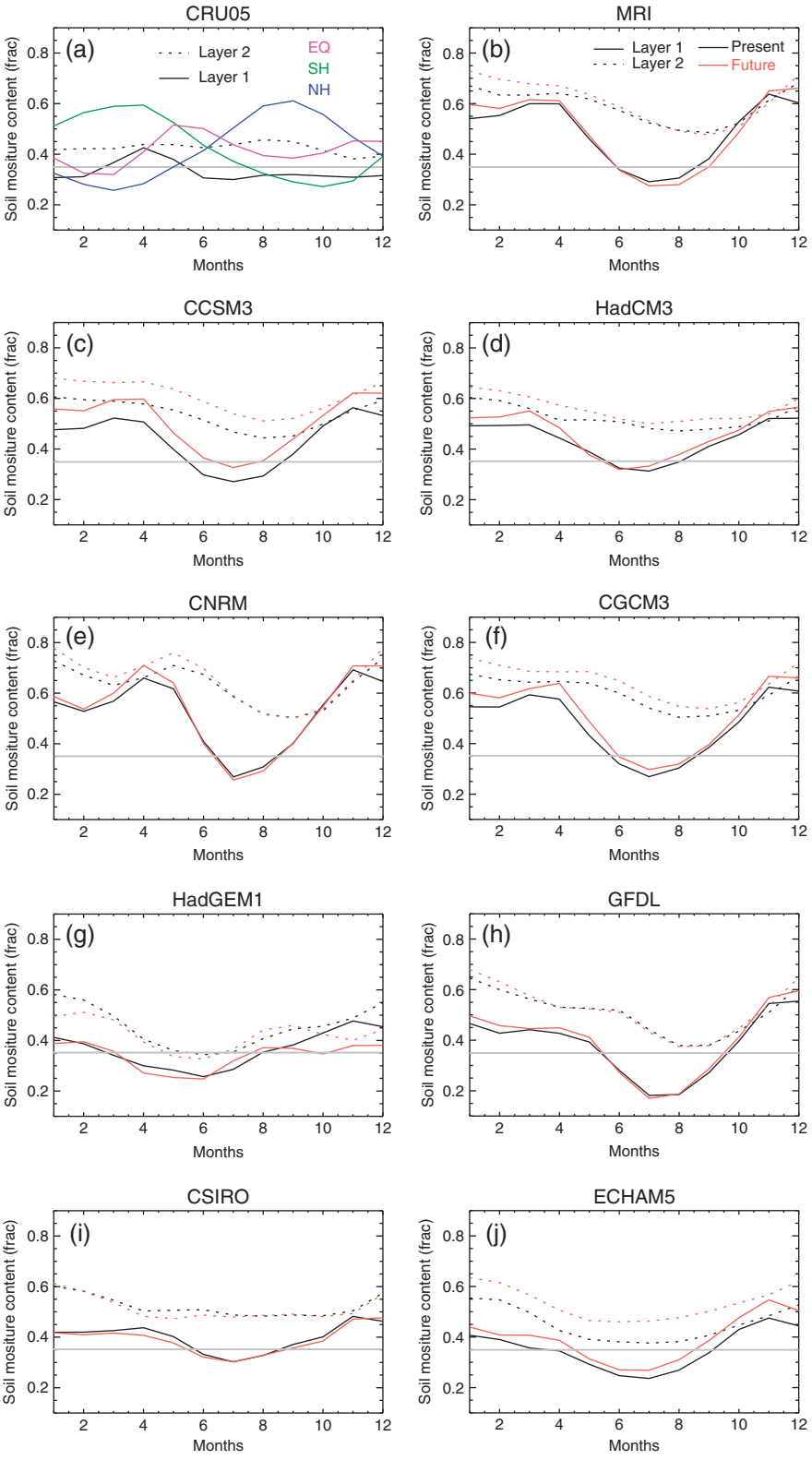
CRU05
(a)
Layer 2
Layer 1
EQ
SH
NH
MRI
(b)
Layer 1
Layer 2
Present
Future
CCSM3
(c)
HadCM3
(d)
CNRM
(e)
CGCM3
(f)
HadGEM1
(g)
GFDL
(h)
CSIRO
(i)
ECHAM5
(j)
Soil mositure content (frac)
Months
0.2
0.4
0.6
0.8
2
4
6
8
10
12

20 mm month^{-1} in the Group 1 and 2 GCMs; not shown) and the dry seasons either wetter for three GCMs (CCSM3, ECHAM5 and CGCM3) or show little change (Fig. 10). Exceptions are HadGEM1 that simulates rainfall decreases in the long rainy season, and MRI/HadGEM1 that simulate small rainfall/soil moisture decreases in parts of the dry season (Fig. 10).

Increased wet season soil moisture, due to increases in rainfall and simulated CO_2-induced reductions in stomatal conductance and evapotranspiration, leads to increases in NPP and hence carbon storage. Seasonality in precipitation and soil water balance are most important for wildfire carbon emissions (C_{fire}). The amount of rainfall, particularly in the wet season, determines the fuel load of biomass and litter, while the length of the fire season determines the fire risk. The length of the fire season in LPJ is defined by the number of days and degree to which the soil moisture is below a threshold for fuel ignition (termed 'moisture of extinction' and shown as approximately the dotted line in Fig. 10) (Thonicke *et al*., 2001). The length of the fire season is greatest for the Groups 3 and 4 GCMs.

The wet Groups 1 and 2 GCMs simulate the lowest annual fire frequencies, i.e. lowest annual area burnt (Table 5). This translates into the lowest C_{fire} for the present-day (Table 4) for the Group 2 GCMs. The Group 1 GCMs simulate high C_{fire} due to the dominant effect of high fuel loads. This is especially the case for MRI. The dry GCM Groups, 3 and 4, generally lead to high-simulated fire frequencies (i.e. the largest annual area burnt), and the largest C_{fire} values (Tables 4 and 5).

Under the future climate, Group 1 and 2 GCMs generally result in the lowest simulated percentage changes in C_{fire} (Table 4) due to high moisture levels The Group 3 simulations exhibit the largest percentage increases in C_{fire}. Simulations driven by HadGEM1, which exhibits future precipitation decreases in the early part of the dry season, show the largest increase both in burnt area and C_{fire}. Although there is variation among GCMs in the sign of the future change in area burnt (Table 5), the absolute differences (Δ values) are small and only the HadGEM1 and CCSM3 results are significantly different (two-sample *t*-test, $P < 0.01$; not shown), reflecting the minor future changes in GCM simulated soil moisture apparent in Fig. 10.

Overall, all GCMs suggest future increases in wet season rainfall that promote NPP and carbon storage. Carbon emissions from wildfires also increase in the future due to (a) increases in simulated NPP which translates into increases in fuel load and (b) a lack of a substantial future change in dry season rainfall amount or timing. Future changes in human induced fires will be affected by demographic trends and practices which are not considered in this study. These will undoubtedly be an important component determining future changes in overall fire related carbon.

Discussion

The LPJ simulation driven by CRU05 climate shows vegetation patterns which are in reasonable agreement with the MODIS/Terra satellite-derived and the GLC 2000 (JRL, 2005) land-cover classifications. Three global land use products, MODIS (Friedl *et al*., 2002), Ramankutty & Foley (1998) and GLC 2000 (JRL, 2005), estimate cropland coverage of 1.8%, 12.5% and 22.7%, respectively, across East Africa in the late 1990s/early 2000s. All three datasets thus agree that natural vegetation covers the majority of the land area in this region. A comparison of forest NPP simulated by LPJ with available plot-based estimates of NPP also shows reasonable agreement. An underestimation of vegetation carbon by LPJ in this comparison may only be partly attributed to the simulation of some grassland areas, which do not occur in the forest plots.

Increases in atmospheric CO_2 concentrations promote increases in simulated NPP and enhanced carbon storage through the CO_2 fertilisation effect (Norby *et al*., 2005; Hickler *et al*., 2008), and increased plant water-use-efficiency in water-limited environments. GCM projections of a warmer, wetter East African climate and enhanced NPP, carbon storage, and runoff lead to an expansion of tropical broadleaved evergreen forest, along with an increase in tropical broadleaved raingreen forest (Fig. 6). In a global simulation study using LPJ, Schaphoff *et al*. (2006) projected increases in future total carbon storage in the region for four out of five GCMs from the IPCC 3rd Assessment Report (Fig. 3 in Schaphoff *et al*., 2006). At the aggregate level, these increases in woody cover are at the expense of tempe-

Fig. 10 Seasonal cycle of soil moisture content averaged over the East African study region region for 1981–2000 under the CRU05 observed climate dataset and the nine GCMs. Solid lines represent soil layer 10–50 cm; dotted lines represents soil layer 250–150 cm. Black lines represent the period 1981–2000 and red lines represent the period 2080–2099. Further coloured lines in (a) also show sub-regional averages for CRU05 for soil layer 1 (NH, north of 3°N – blue solid line; SH, south of 3°NS – green solid line; EQ, equatorial regions bounded by 3°N–3°S – pink solid line) Soil moisture content is expressed as a fraction over the 150 cm LPJ soil column. A value of zero represents wilting point, and one field capacity. The moisture of extinction of 0.35 is plotted in grey; below this value the ecosystems are more vulnerable to fire (note, the moisture of extinction is not a strict cutoff for fire as the probability of fire occurrence is not a step-function in Thonicke *et al*., 2001).

rate forest cover and C_4 and C_3 grasslands, which in a few locations (Fig. 8) are large enough to change the dominant plant type. Our results generally also agree with those of from the global multi-GCM, multi-emissions scenario LPJ driven simulations of Scholze *et al*. (2006), in simulating (their Fig. 2) future increases in runoff and woody coverage (but not biome shifts), and equivocal future changes in wildfire frequency across East Africa. Qualitatively our results agree with sensitivity simulations by Hély *et al*. (2006) that suggest present-day biomes of Central Africa to be insensitive to precipitation increases.

There are several uncertainties and limitations with the current analysis. Firstly, this study presents regional projections of changes in NPP and carbon storage given one future climate forcing scenario – the SRES A2 emissions scenario. However, in LPJ simulations driven by climate projections from multiple SRES scenarios, Sitch *et al*. (2008) showed generally similar but weaker ecosystem responses as the scenarios became less extreme. Moreover, the ranges of uncertainty in ecosystem responses associated with multi-GCM scenarios (using LPJ forced with nine GCM climates) presented in this study are larger than the corresponding LPJ uncertainty ranges arising from the use of four different SRES multi-emissions scenarios and one GCM (Sitch *et al*. (2008), as shown in Table 6. As discussed in 'Materials and methods', A2 represents among the strongest greenhouse forcing among the IPCC SRES emissions scenarios, yet the simulations in this study do not generally suggest that increases in water stress of significance for natural vegetation will occur, despite the considerably warmer future temperatures. One reason for this is the decreased stomatal conductance simulated by the model under higher CO_2 concentrations (Hickler *et al*., 2006), which is consistent with experimental observations for many plant species (Medlyn *et al*., 2001; Poorter & Navas, 2003). A second limitation to our analysis is that East Africa is a region of complex topography (high elevation areas, large lakes and wetlands), which induce localised climatic patterns with heterogeneous associated vegetation (McHugh, 2005); unfortunately future changes in such patterns cannot be fully captured at the coarse resolution of GCMs – even though a number of these are now applied at a fine enough resolution to resolve the Great Lakes (Fig. 5). Our results are applicable in terms of the broad, regional patterns but not necessarily the finer spatial detail. Lastly, the version of LPJ we used does not deal with a number of important processes that may substantially affect carbon balance in the Central/East African region in the future. In particular, human land-use and its effects on vegetation structure and function have not been considered (Zaehle *et al*., 2007), nor possible phosphorous or nitrogen limitation (Vitousek & Howarth, 1991).

Implications for ecosystem services

As noted by Scholze *et al*. (2006), future climate-induced changes in land cover will occur concurrently with human-induced changes in land use, and in general, human-driven transitions may have larger impacts on ecosystems than transitions associated only with climate shifts. The impact of changes in climate and land use will be felt in agriculture, which will continue to play a crucial role in most countries of the region through its direct and indirect impacts on rural development and patterns of migration (Scholes & Biggs, 2004; DFID, 2005). Further pressures will arise from population increases. Recent projections for six countries of the study region (Ethiopia, Rwanda, Burundi, Uganda, Kenya, and Tanzania) indicate a near-trebling in the number of people between 2000 and 2050, from 174 to 498 million (UNPD, 2008). At the same time, populations are urbanising rapidly, and although income

Table 6 Absolute and percentage change in carbon fluxes and pools across East Africa between the periods 1980–1999 and 2080–2099 from this multi-GCM study (using LPJ forced with nine GCM climatologies) and those from Sitch *et al*. (2008) for simulations performed with LPJ forced with one GCM and 4 SRES emission scenarios

Variable	Multi-GCM driven range (this study) – Mmod		Multi-emissions scenario range with HadCM3 (Sitch *et al*., 2008) – Memis		Comparison, this multi-GCM study (Mmod) vs four SRES emissions scenarios with one GCM model (Memis)
Carbon fluxes	Δ (g C m^{-2} yr^{-1})	%	Δ (g C m^{-2} yr^{-1})	%	Δ (g C m^{-2} yr^{-1})
NPP	153–314	18–36	130–282	16–34	Similar
NEE	−40 to 47	↑ ↓	−10 to −28	↓	Mmod > Memis
C_{fire}	3–59	3–58	23–28	29–35	Mmod > Memis
Carbon pools	Δ (kg C m^{-2})	%	Δ (kg C m^{-2})	%	Δ (kg C m^{-2})
VegC	1.2–3.3	9–22	2.8–3.7	28–38	Mmod > Memis
SoilC	−0.6 to + 0.3	0 to −8	−0.6 to −0.7	−7 to −8	Mmod > Memis

growth in the region is slow, demand for agricultural products, livestock products and wood for fuel is rising rapidly and the trends are likely to continue for the foreseeable future (FAO, 2006).

As discussed above, the version of the LPJ model used in this study does not take account of human-driven changes in land cover, but the simulation results, in combination with other findings for the region, do allow some conclusions concerning the possible future impacts on ecosystem goods and services, in particular water and food security in terms of agricultural production. The LPJ results concerning freshwater availability in the region are reasonably consistent, with only one GCM leading to a projected decrease in runoff (Table 5). The mean change in runoff across the simulations is $+94\,\mathrm{mm\,yr^{-1}}$ (Table 5) or a 19% increase in 2080–2100 compared with 1981–2000. Increasing runoff may increase the availability of freshwater in the region, although it also carries the possibility of increased flood risk in flood-prone areas and of increased soil erosion on sloping lands. There is also the possibility of increased pathogen loads in areas that do not have good water supply and sanitation infrastructure (IPCC, 2007).

The decreases that are projected in grass cover (Fig. 6) in 2080–2100 compared with 1981–2000; not shown) may have potentially serious implications for pastoralism in the region. Pastoralists are currently also faced with competition for land from wildlife as well as from human settlement and cropland expansion (Hobbs *et al*., 2008). With decreases in grassland coverage they may be faced with fewer options for accessing dry-season feeding resources. At the same time, the projected increases in carbon storage in the region (3–13%) may present new opportunities for livestock keepers in extensive grazing systems in the form of payment for carbon sequestration in vegetation and soils. These opportunities also bring challenges, however, related to incentive systems, institutional linkages, policy reforms, monitoring techniques for carbon stocks, and appropriate verification protocols (Reid *et al*., 2004).

Two crops that are grown widely in this region are maize and *Phaseolus* beans. Maize is a C_4 crop and is therefore more tolerant of higher temperatures compared with the C_3 beans (Jones & Thornton, 2003; Thornton *et al*., 2009). Medium-to-high altitude areas in the region are generally below the optimal annual–average temperature range for tropical (30–35 °C) and tropical highland (20–30 °C) maize varieties (FAO, 1978). For beans, yields have been shown to decline above 20–22° (Thornton *et al*., 2009). These temperature ranges for maize and beans are plotted alongside LPJ-derived PFT ranges in Fig. 9. All the GCM projections suggest that tropical maize will still thrive in the 2080–2100 period as average temperatures increase, but in many of these environments, water limitations may induce yield declines (Thornton *et al*., 2009). Optimal temperatures of highland maize varieties at the lower-end of the 20–30 °C range and beans are only $\sim$ 2–4 °C higher than maximum temperature limits for temperate trees which decline substantially or disappear toward the end of the 21st century in all simulations (Figs 7 and 9). The warmest GCMs, Groups 1 and 4, project annual-mean temperatures in 2080–2100 to exceed 22 °C in the majority of grid-cells, (Fig. 9). Hence only in the deciduous forest grid cells with annual-mean temperatures <22 °C will beans and low-temperature tolerant highland tropical maize varieties continue to thrive in the climatic futures projected by these GCMs. Overall, alongside projections of increased productivity for natural vegetation, our study suggests potential increases for tropical maize food production in situations where water availability is not limiting. However, tropical highland maize and bean production is likely to decline in a warmer future climate. Shifts in yields may have important impacts on householders' incomes and food security.

Several crop modelling studies that have assessed the agricultural impacts of projected changes in future climate in the region suggest overall yield declines. Parry *et al*. (2004) indicate that cereal yields in East Africa may decrease by 5–20% by the 2090s, depending on emission scenario; Lobell *et al*. (2008) suggest an overall 5% decrease in maize and bean production in East Africa by 2030. Thornton *et al*. (2009) suggest aggregate losses of 5–15% of current regional production of both maize and beans to the 2050s, depending on emission scenario used, with highland areas experiencing yield increases and low elevation areas yield decreases. Decreases in bean yields in the region and maize yields in medium-to-high altitude areas are attributed primarily to temperature stress, while in lower elevation areas maize decreases are associated with climate-induced water stress (Thornton *et al*., 2009). Hence average temperature is not the main driver of yield change in the low-elevation maize growing pixels analysed. This water-stress effect is at first sight contrary to our simulated results. The GCMs and emissions scenario considered generally project rainfall increases, as do the projections used by Thornton *et al*. (2009) and hence little water stress is inferred in our study (Figs 9 and 10). However, unlike the crop models applied in Thornton *et al*. (2009), LPJ incorporates physiological effects of elevated CO_2 which leads to direct stimulation of plant productivity and indirect stimulation through increases in plant water-use-efficiency (WUE) in natural ecosystems in response to increased CO_2. This acts towards reducing water limitation as atmospheric CO_2 concentrations increase and

the climate warms. However, the degree to which such enhancements will apply to crops, especially maize and other crops with the C_4 photosynthetic pathway, is unclear (Long *et al.*, 2006). Tropical maize will only benefit indirectly from elevated CO_2 through increased WUE (Long *et al.*, 2006) and in general from greater regional water availability.

To summarise, although LPJ results suggest increases in NPP during this century, results from other work suggest that these increases may not be translated into increases in agricultural potential or in crop yields (at least, with current crop genetic material), primarily because of temperature stresses, e.g. increased plant respiration and increases in crop development rates with warming (Lobell & Field, 2007; Thornton *et al.*, 2008). At an aggregated level, the changing climate may have relatively muted impacts on food production in East Africa. Local impacts in some highland regions could even bring opportunities for increased production or crop diversification. However, local impacts for some croppers and pastoralists are likely to compound existing problems of poverty and vulnerability.

In conclusion, East Africa is one of few tropical regions where GCMs generally agree on a strong future warming and rainfall increases in most seasons (e.g., Hulme *et al.*, 2001; Christensen *et al.*, 2007). In terms of the magnitude of carbon cycle responses to a range of future climate projections, the GCMs could be grouped into four broad categories which relate their climate to that of the GCM average. (1) Warmer, wetter GCMs with large positive future temperature and rainfall trends produce the largest increases in NPP and total carbon storage. (2) Cooler, wetter GCMs with large positive future temperature and rainfall trends which produce the next largest increases in NPP and carbon storage. (3) Fairly warm and dry GCMs with strong positive future trends in rainfall which yield minor NPP and carbon storage trends. (4) A warmer, drier GCM with strong future trends in temperature or rainfall produced an outlier in terms of ecosystem response, with little future trend in vegetation, NPP or carbon balance. In terms of seasonality, all GCMs suggest wet seasons becoming wetter in the future, promoting NPP and carbon storage, while changes in dry season rainfall or soil moisture amounts are small. Projected climate translates into relatively consistent projections of change in vegetation towards more tree-dominated ecosystems and a positive ecosystem carbon balance across East Africa towards the end of the 21st century, with potential benefits for ecosystem services. Increased rainfall, river runoff and fresh water availability alongside enhanced NPP may be tentatively expected to improve conditions for agriculture, provided temperature is not a limiting factor.

Acknowledgements

We thank three anonymous reviewers for their helpful suggestions. We also thank Sibyll Schaphoff and Dieter Gerten for providing the LPJv1.2 model code and for helpful discussions. We acknowledge the GCM modelling groups for providing their data for analysis, the Program for Climate Model Diagnosis and Intercomparison (PCMDI) for collecting and archiving the model output, and the JSC/CLIVAR Working Group on Coupled Modelling (WGCM) for organising the model data analysis activity. The multi-model data archive is supported by the Office of Science, U.S. Department of Energy. MODIS/Terra land use data were obtained courtesy of NASA. This research has been partly funded as part of the National Science Foundation Biocomplexity of Coupled Human and Natural Systems Program, Award Number BCS 0308420, and Michigan State University, USA. S. S. was supported by the UK DEFRA Climate Prediction Programme under Contract PECD 7/12/37. B.S. acknowledges support from the Swedish Research Council Formas and Mistra-SWECIA. We thank Andrew Marshall, Jon Lovett and the Valuing the Arc team, supported by a Leverhulme Program Grant, for access to inventory data and a NERC New Investigators Award to S.L.L. for funding some of the plot data collection work. S.L.L. is supported by a Royal Society University Research Fellowship.

References

Berthelot M, Friedlingstein P, Ciais P, Dufresne J-L, Monfray P (2005) How uncertainties in future climate change predictions translate into future terrestrial carbon fluxes. *Global Change Biology*, **11**, 959–970.

Chave J, Andalo C, Brown S *et al.* (2005) Tree allometry and improved estimation of carbon stocks and balance in tropical forests. *Oecologia*, **145**, 87–99.

Chave J, Coomes D, Jansen S, Lewis SL, Swenson NG, Zanne AE (2009) Towards a worldwide wood economics spectrum. *Ecology Letters*, **12**, 351–366.

Christensen JH, Hewitson B, Busuioc A *et al.* (2007) Regional climate projections. In: *Climate Change 2007: The Physical Science Basis. Contribution of Working Group I to the Fourth Assessment Report of the Intergovernmental Panel on Climate Change* (eds Solomon S, Qin D, Manning M, Chen Z, Marquis M, Averyt KB, Tignor M, Miller HL), Cambridge University Press, Cambridge, UK.

Conway D (2002) Extreme rainfall events and lake level changes in East Africa: recent events and historical precedents. In: *The East African Great Lakes: Limnology, Palaeolimnology and Biodiversity* (eds Odada EO, Olago DO), pp. 63–92. Kluwer, Dordrecht, The Netherlands.

Cox PM, Betts RA, Collins M, Harris PP, Huntingford C, Jones CD (2004) Amazonian forest dieback under climate-carbon cycle projections for the 21st century. *Theoretical and Applied Climatology*, **78**, 137–156.

Cox PM, Betts RA, Jones CD, Spall SA, Totterdell IJ (2000) Acceleration of global warming due to carbon-cycle feedbacks in a coupled climate model. *Nature*, **408**, 184–187.

Cramer W, Bondeau A, Schaphoff S, Lucht W, Smith B, Sitch S (2004) Tropical forests and the global carbon cycle: impacts of atmospheric CO_2, climate change and rate of deforestation. *Philosophical Transactions of the Royal Society B*, **359**, 331–343.

Cramer W, Bondeau A, Woodward FI *et al*. (2001) Global response of terrestrial ecosystem structure and function to CO_2 and climate change: results from six dynamic global vegetation models. *Global Change Biology*, **7**, 357–373.

Deans JD, Moran J, Grace J (1996) Biomass relationships for tree species in regenerating semi-deciduous tropical moist forest in Cameroon. *Forest Ecology and Management*, **88**, 215–225.

Denman KL, Brasseur G, Chidthaisong A *et al*. (2007) Couplings between changes in the climate system and biogeochemistry. In: *Climate Change 2007: The Physical Science Basis. Contribution of Working Group I to the Fourth Assessment Report of the Intergovernmental Panel on Climate Change* (eds Solomon S, Qin D, Manning M, Chen Z, Marquis M, Averyt KB, Tignor M, Miller HL), Cambridge University Press, Cambridge, UK.

Department for International Development (DFID) (2005). DFID's Draft Strategy for Research on Sustainable Agriculture (SRSA) 2006–2016. 15 pp.

Etheridge DM, Steele LP, Langenfelds RL *et al*. (1996) Natural and anthropogenic changes in atmospheric CO2 over the last 1000 years from air in Antarctic ice and firn. *Journal of Geophysical Research*, **101**, 4115–4128.

FAO (1978) *Report on the Agro-Ecological Zones Project. World Soil Resources Report 48*. United Nations Food and Agriculture Organisation (FAO), Rome.

FAO (1991) *The Digitized Soil Map of the World (Release 1.0). Vol. 67/1*. Food and Agriculture Organization of the United Nations.

FAO (2006) *World Agriculture: Towards 2030/2050*. Interim report, Global Perspective Studies Unit, Food and Agriculture Organization of the United Nations, Rome, Italy.

Friedl MA, McIver DK, Hodges JCF *et al*. (2002) Global land cover from MODIS: algorithms and early results. *Remote Sensing of Environment*, **83**, 135–148.

Friedlingstein P, Cox P, Betts R *et al*. (2006) Climate-carbon cycle feedback analysis: results from the C4MIP model intercomparison. *Journal of Climate*, **19**, 3337–3353.

Gerten D, Schaphoff S, Haberlandt U, Lucht W, Sitch S (2004) Terrestrial vegetation and water balance: hydrological evaluation of a dynamic global vegetation model. *Journal of Hydrology*, **286**, 249–270.

GRUMP (The Global Rural-Urban Mapping Project) (2005). GRUMP Alpha version. Available at http://www.ciesin.columbia.edu/download_data.html

Hély C, Bremond L, Alleaume S, Smith B, Sykes MT, Guiot J (2006) Sensitivity of African biomes to changes in the precipitation regime. *Global Ecology and Biogeography*, **15**, 258–270.

Hickler T, Prentice IC, Smith B, Sykes MT, Zaehle S (2006) Implementing plant hydraulic architecture within the LPJ Dynamic Global Vegetation Model. *Global Ecology and Biogeography*, **15**, 567–577.

Hickler T, Smith B, Prentice IC, Mjöfors K, Miller P, Arneth A, Sykes MT (2008) CO_2 fertilization in temperate forest FACE experiments not representative of boreal and tropical forests. *Global Change Biology*, **14**, 1.12.

Hobbs NT, Galvin KA, Stokes CJ *et al*. (2008) Fragmentation of rangelands: implications for humans, animals, and landscapes. *Global Environmental Change*, **18**, 776–785.

Hulme M, Doherty R, Ngara T (2001) African climate change: 1900–2100. *Climate Research*, **17**, 145–168.

IPCC (2001) *Climate Change 2001: The Scientific Basis*, Houghton J. ed., Cambridge University Press, Cambridge, UK.

IPCC (Intergovernmental Panel on Climate Change) (2007). Climate Change 2007: Impacts, Adaptation and Vulnerability. Summary for policy makers.

Jones PG, Thornton PK (2001) *Bimodal Rainfall Areas of Africa*. CIAT GIS Unit digital data set, Cali, Colombia.

Jones PG, Thornton PK (2003) The potential impacts of climate change in tropical agriculture: the case of maize in Africa and Latin America in 2055. *Global Environmental Change*, **13**, 51–59.

JRL (2005). GLC 2000 (global land cover) data layer, Joint Research Laboratory, Ispra, Italy. Available at http://bioval.jrc.ec.europa.eu/products/glc2000/glc2000.php (accessed 8 December 2008).

Keeling CD, Whorf TP, Wahlen M *et al*. (1995) Interannual extremes in the rate of rise of atmospheric carbon dioxide since 1980. *Nature*, **375**, 666–670.

Lewis SL (2006) Tropical forests and the changing Earth System. *Philosophical Transactions of the Royal Society B*, **361**, 195–210.

Lewis SL, Lopez-Gonzalez G, Sonké B *et al*. (2009) Increasing carbon storage in intact African tropical forests. *Nature*, **457**, 1003–1007.

Lobell DB, Burke MB, Tebaldi C, Mastrandrea MD, Falcon WP, Naylor RL (2008) Prioritizing climate change adaptation needs for food security in 2030. *Science*, **319**, 607–610.

Lobell DB, Field CB (2007) Global scale climate-crop yield relationships and the impact of recent warming. *Environmental Research Letters*, **2**, 014002, doi: 10.1088/1748-9326/2/1/014002.

Long SP, Ainsworth EA, Leakey ADB, Nösberger J, Ort DR (2006) Food for thought: lower-than-expected crop yield stimulation with rising CO_2 concentrations. *Science*, **312**, 1918–1921.

McHugh MJ (2005) Multi-model trends in East African rainfall associated with increased CO_2. *Geophysical Research Letters*, **32**, L01707, doi: 10.1029/2004GL021632.

Medlyn BE, Barton CVM, Broadmeadow MSJ *et al*. (2001) Stomatal conductance of forest species after long-term exposure to elevated CO2 concentration: a synthesis. *New Phytologist*, **149**, 247–264.

Morales P, Sykes MT, Prentice IC *et al*. (2005) Comparing and evaluating process-based ecosystem model predictions of carbon and water fluxes in major European forest biomes. *Global Change Biology*, **11**, 2211–2233.

Nakicenovic N, Swart R (eds) (2000) *Special Report on Emissions Scenarios*. Cambridge University Press, Cambridge, UK.

New MG, Hulme M, Jones PD (2000) Representing twentieth century space-time climate variability. Part II: development of 1901–1996 monthly grids of terrestrial surface climate. *Journal of Climate*, **13**, 2217–2238.

Norby RJ, DeLucia EH, Gielen B *et al*. (2005) Forest response to elevated CO_2 is conserved across a broad range of productivity. Proceedings of the National Academy of Sciences, USA, **102**, 18052–18056.

Parry ML, Rosenzweig C, Iglesias A, Livermore M, Fischer G (2004) Effects of climate change on global food production under SRES emissions and socio-economic scenarios. *Global Environmental Change*, **14**, 53–67.

Poorter H, Navas M-L (2003) Plant growth and competition at elevated CO_2: on winners, losers and functional groups. *New Phytologist*, **157**, 175–198.

Ramankutty N, Foley JA (1998) Characterizing patterns of global land use: an analysis of global croplands data. *Global Biogeochemical Cycles*, **12**, 667–685.

Reid RS, Thornton PK, McCrabb GJ, Kruska RL, Atieno F, Jones PG (2004) Is it possible to mitigate greenhouse gas emissions in pastoral ecosystems of the tropics? *Environment, Development and Sustainability*, **6**, 91–109.

Ruosteenoja K, Carter TR, Jylhä K, Tuomenvirta H (2003) *Future Climate in World Regions: And Intercomparison of Model-Based Projections for the New IPCC Emissions Scenarios*. Finnish Environment Institute, Helsinki.

Schaphoff S, Lucht W, Gerten D, Sitch S, Cramer W, Prentice IC (2006) Terrestrial biosphere carbon storage under alternative climate projections. *Climatic Change*, **74**, 97–122.

Scholes RJ, Biggs R (eds) (2004). Ecosystem services in southern Africa: a regional assessment. Millennium Ecosystem Assessment. Available at http://www.millenniumassessment.org/en/SGA.Safma.aspx

Scholze M, Knorr W, Arnell NW, Prentice IC (2006) A climate-change risk analysis for world ecosystems. *Proceedings of the National Academy of Science*, **103**, 13116–13120.

Sitch S, Huntingford C, Gedney N (2008) Evaluation of the terrestrial carbon cycle, future plant geography, and climate-carbon cycle feedbacks using 5 Dynamic Global Vegetation Models (DGVMs). *Global Change Biology*, **14**, 1–25, doi: 10.1111/j.1365-2486.2008.01626.x.

Sitch S, Smith B, Prentice IC *et al*. (2003) Evaluation of ecosystem dynamics, plant geography and terrestrial carbon cycling in the LPJ Dynamic Vegetation Model. *Global Change Biology*, **9**, 161–185.

Thonicke K, Venevsky S, Sitch S, Cramer W (2001) The role of fire disturbance for global vegetation dynamics: coupling fire into a Dynamic Global Vegetation Model. *Global Ecology and Biogeography*, **10**, 661–677.

Thornton PK, Jones PG, Alagarswamy A, Andresen K (2009) Spatial variation of crop yield responses to climate change in East Africa. *Global Environmental Change*, **19**, 54–65.

UNPD (2008). Population Division of the Department of Economic and Social Affairs of the United Nations Secretariat, World Population Prospects: The 2006 Revision and World Urbanization Prospects: The 2005 Revision. Available at http://esa.un.org/unpp (September 2008).

Vitousek PM, Howarth RW (1991) Nitrogen limitation on land and in the sea: how can it occur? *Biogeochemistry*, **13**, 87–115.

Zaehle S, Bondeau A, Carter TR *et al*. (2007) Projected change in terrestrial carbon storage in Europe under climate and land use change. *Ecosystems*, **10**, 380–401.

Zaehle S, Sitch S, Smith B, Hatterman F (2005) Effects of parameter uncertainties on the modeling of terrestrial biosphere dynamics. *Global Biogeochemical Cycles*, **19**, GB3020, doi: 10.1029/2004GB002395.

Zobler L (1986) A world soil file for global climate modelling. NASA Technical Memorandum, 87802, 32 pp.